Evolution of N-body Kepler systems with gravitational scatterings and merges of bodies by direct collision

Frank de Jongh

(5175836)

BSc thesis, Technische Wiskunde +
Technische Natuurkunde
Technische Universiteit Delft

Delft, 21 August 2025

Supervising Teachers: Dr. P.M. Visser,
Dr. S.W.H. Eijt

Abstract

This thesis studies the evolution of N-body Keplerian systems (N=500) using an algorithm [11] developed by P.M. Visser that mathematically predicts when a close encounter occurs. It attempts to address 3 questions: (1) The influence of the spread in orbital eccentricities on the number of scatterings $n_{\max}$ required for a stable system, (2) the time dependence of the number of scatterings $n_{\text{scatt}}(t)$ (3) predicting the number of scatterings $n_{\max}$ required for a system to reach a stable configuration in which no more scatterings occur. Simulations show that as $\epsilon_{\max}$ increases, $n_{\max}$ also increases. The relative uncertainty in $n_{\max}$ also decreases as $\epsilon_{\max}$ increases, indicating randomness playing less of a role for higher eccentricities. The results also indicate that there is a relation between n_{scatt} and t that very accurately describes the evolution of systems throughout time defined by $n_{\text{scatt}}(t) = n_{\max} - ae^{-t/\tau}$ which can be rewritten as $n_{\text{scatt}}(t) = n_{\max}\left(1 - e^{(t-t_0)/\tau}\right)$. Here, t_0 is a time offset in years, and τ is the timescale of the system, also given in years. This formula accurately describes every single simulation ran in this paper, increasing in accuracy as $n_{\max}$ increases. Finally, no clear method was found to predict the number of scatterings $n_{\max}$ needed for a system to become stable. This is due to the chaotic nature of the system, where very small changes in initial conditions cause massively different outcomes. Because 500 planets interact with each other, mutating each other's orbits, a very small change can result in different planets colliding at different times. These planets then in turn also collide with other planets, quickly diverging from other initial conditions. The paper discusses limitations of the algorithm, such as a lack of conservation of momentum and energy and an arbitrary cutoff for the fitted function. This research aims to further implement the algorithm [11] developed by P.M. Visser and simulate systems until they become practically stable, after which the result of many gravitational and direct scatterings can be analyzed in detail.

Table of Contents

Abstract ii

1 Introduction 1

2 Theory 3
- 2.1 Kepler Orbits . . . 3
- 2.2 Gravitational sphere of influence . . . 4
- 2.3 Elastic collisions using hyperbolic orbit . . . 6
- 2.4 Direct inelastic collisions between bodies . . . 7
- 2.5 Effect of the Sun's gravitational pull during close encounter . . . 8
- 2.6 Initial state: a flat circular disk . . . 8

3 Simulation Method 11
- 3.1 Initialization . . . 11
- 3.2 Main loop of the algorithm . . . 12
- 3.3 Scattering Detection . . . 12
  - 3.3.1 Determining scattering pairs . . . 12
  - 3.3.2 Calculating the time of a scattering . . . 13
- 3.4 Performing a close encounter event . . . 14
  - 3.4.1 Before scatter event . . . 14
  - 3.4.2 The scatter event . . . 14
  - 3.4.3 After scatter event . . . 15
- 3.5 Finding new scattering possibilities . . . 15

4 Results 16
- 4.1 Maximum eccentricity of 0.1 . . . 16
- 4.2 Maximum eccentricity of 0.2 . . . 21
- 4.3 Maximum eccentricity of 0.4 . . . 26
- 4.4 Comparing different values for $e_{\max}$ . . . 31

5 Discussion 33

6 Conclusion 36

References 37

1 Introduction

A Keplerian system describes any system in space where the objects in said system follow the planetary laws of motion derived by the astronomer Johannes Kepler in the 17th century. These laws assume that all objects orbit a central stationary body, as is the case in our Solar System. Said objects can be various celestial objects such as moons, stars, planets or comets. These celestial objects of course also interact with each other through gravity, influencing each other's orbit. By studying these Keplerian systems, we can not only predict the evolution of these systems and it's respective objects, but also deduce how the system evolved to its current state. This will further our understanding of the formation and evolution of our own Solar System. As described in the previous paragraph, the laws of Kepler assume that an object is orbiting a central mass, neglecting the gravitational pull between other objects. This simplification is based on the assumption that the gravitational pull of the central mass is much larger than the gravitational pull between the other objects. However, as objects get very close to each other, this assumption does not always hold up. Due to the chaotic N-body nature of these systems, small deflections in just a single object's orbit can significantly affect the evolution of said system. Therefore we are interested in a simulation where gravitational forces between all objects are taken into account.

In this research, we will combine and expand upon the code of previous studies by Jort Koks [9] and Martijn Moorlag [6], who implemented gravitational scatterings and direct collisions respectively. A gravitational scattering is an elastic interaction between two bodies where they get close enough to each other to alter each other's orbits, whereas a direct collision is an inelastic interaction in which two bodies collide and merge to form a new body. Both studies use the same algorithm [11] to detect when a scattering occurs, which can then either be a direct collision or gravitational scattering. The cases are treated separately within the code. N-body systems will be randomly generated according to a set of parameters, where the maximum eccentricity $\epsilon_{max} \in \{0.1, 0.2, 0.4\}$ is varied between simulations, limiting ourselves to realistic values for asteroid belts such as the Kuiper belt as can be seen in Figure 1.1. The systems will have a homogeneous disk of particles and a mass distribution similar to those found in asteroid belts.

Since both studies [9] [6] did not run the algorithm until the systems become effectively stable, we will be attempting to answer a few questions related to the evolution from an initial system to its effectively stable final state. The questions are as follows:

1. *How does the total amount of scatterings n_{max} needed for a system to become effectively stable relate to the maximum eccentricity ϵ_{max}?*
2. *Is the total amount of occurred scatterings n_{scatt} related to the elapsed time t? If so, can we find a general closed form formula $n_{scatt}(t)$ to fit the data?*
3. *Can the total amount of scatterings required for practical stability n_{max} be predicted based on the simulation parameters?*

Chapter 2 of this thesis will explain the existing theory of Kepler's laws of motion, Newtonian gravity and the theory related to the algorithm used to detect and simulate interplanetary interactions. Chapter 3 will describe the initialization of the generated systems and the theory behind the main loop of the algorithm. Chapter 4

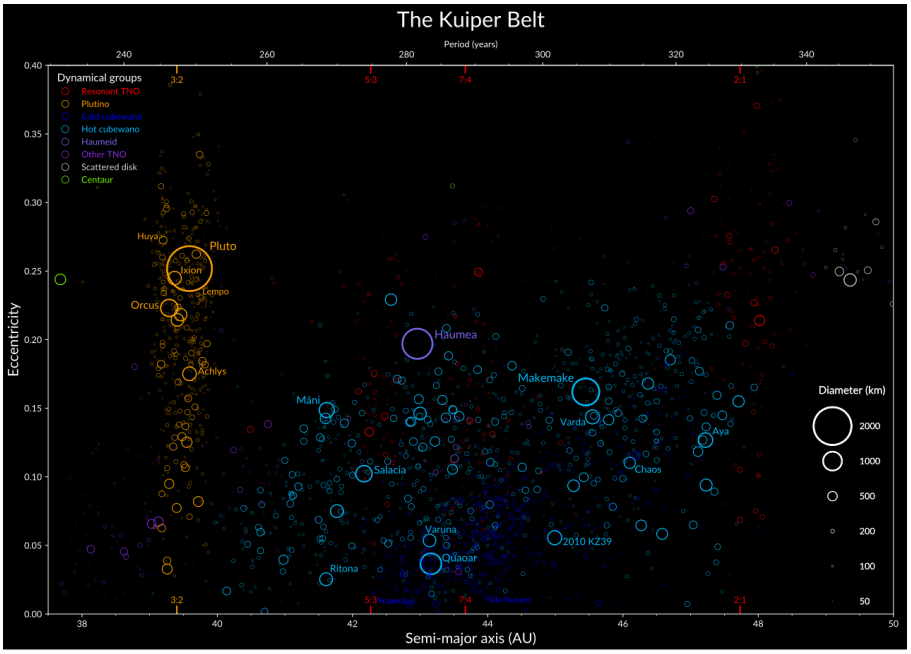

Figure 1.1: Semi-major axis in astronomical units AU versus eccentricity structure of the Kuiper belt. Note the value of $\epsilon_{\max}$ that can be observed. [10]

will showcase the results obtained by the simulations. The results will then further be discussed in Chapter 5. Finally, in chapter 6 the thesis will be concluded by summing up the important outcomes and their consequences. This thesis is part of the BSc programme Applied Mathematics and Applied Physics of the Delft University of Technology.

2

Theory

In the following chapters we will discuss the theory required to properly discuss Visser's algorithm [11] with gravitational scatterings and direct collisions.

2.1. Kepler Orbits

Kepler orbits describe the motion of a body relative to a body that is assumed to be stationary. This stationary assumption holds when the mass of the orbiting planet is much smaller than the central mass, so for example the Earth compared to the Sun. Another example would be the asteroid belt between Mars and Jupiter. Keplerian orbits of a body can be described completely through its angular momentum $\boldsymbol{L}$, eccentricity $\boldsymbol{\epsilon}$, mass m and semi-major axis a. Here $\boldsymbol{\epsilon}$ has magnitude ϵ and points from the center of the orbit towards the closest point of approach of the central body, also known as the periapsis. From $\boldsymbol{L}$ and $\boldsymbol{\epsilon}$, we can determine the 5 conserved orbital parameters: the semi-major axis a, the eccentricity ϵ, the argument of periapsis $\overline{\omega}$, longitude of the descending node Ω, and the inclination I (See figure 2.1).

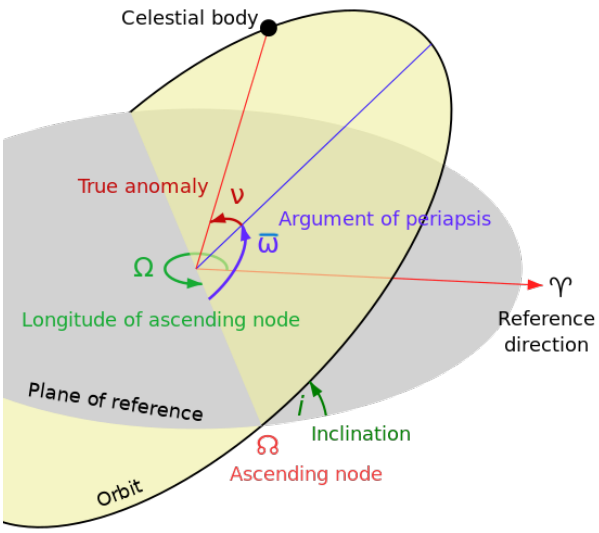

Figure 2.1: Diagram showing the orbital parameters [7]

The equations to determine the remaining 5 orbital parameters are as follows, where $\mathscr{R}$ is a constant rotation matrix [11]:

$$\boldsymbol{L} = L\mathscr{R}\begin{pmatrix}0\\0\\1\end{pmatrix} = L\begin{pmatrix}\sin\Omega\sin I\\-\cos\Omega\sin I\\\cos I\end{pmatrix} \tag{2.1}$$

$$\boldsymbol{\epsilon} = \epsilon\mathscr{R}\begin{pmatrix}1\\0\\0\end{pmatrix} = \epsilon\begin{pmatrix}\cos\overline{\omega}\cos\Omega-\sin\overline{\omega}\sin\Omega\cos I\\\cos\overline{\omega}\sin\Omega+\sin\overline{\omega}\sin\Omega\cos I\\\sin\overline{\omega}\sin I\end{pmatrix} \tag{2.2}$$

$$\mathscr{R} = \begin{pmatrix}\cos\Omega&-\sin\Omega&0\\\sin\Omega&\cos\Omega&0\\0&0&1\end{pmatrix}\begin{pmatrix}1&0&0\\0&\cos I&-\sin I\\0&\sin I&\cos I\end{pmatrix}\begin{pmatrix}\cos\overline{\omega}&-\sin\overline{\omega}&0\\\sin\overline{\omega}&\cos\overline{\omega}&0\\0&0&1\end{pmatrix} \tag{2.3}$$

We can find L through the equations $L = m\omega ab$, where $\omega = \sqrt{\frac{GM_\odot}{a^3}}$ and $b = a\sqrt{1-\epsilon^2}$. From L_3 in equation 2.1 we can find I, which we can then use to deduce Ω from either L_1 or L_2. Finally, to determine $\overline{\omega}$, we can look at equation 2.2 to deduce it from ϵ_3.

The orbit is parametrized by the true anomaly ν or the eccentric anomaly $\overline{E}$. The position vector and the velocity vector can now be expressed as follows:

$$\boldsymbol{r} = \begin{pmatrix}x\\y\\z\end{pmatrix} = r\mathscr{R}\begin{pmatrix}\cos\nu\\\sin\nu\\0\end{pmatrix} = \mathscr{R}\begin{pmatrix}a\cos\overline{E}-c\\b\sin\overline{E}\\0\end{pmatrix} \tag{2.4}$$

$$\boldsymbol{v} = \dot{\boldsymbol{r}} = \frac{\omega a}{b}\begin{pmatrix}-a\sin\nu\\a\cos\nu+c\\0\end{pmatrix} = \frac{\omega a}{r}\mathscr{R}\begin{pmatrix}-a\sin E\\b\cos E\\0\end{pmatrix} \tag{2.5}$$

Finally, we use Kepler's equation to describe the relation between the eccentric anomaly $\overline{E}$, mean anomaly $\overline{M}$ and the time t since periapsis:

$$\overline{M} = \omega t = \overline{E} - \sin\overline{E} \Leftrightarrow t = \frac{\overline{E}-\sin\overline{E}}{\omega} \tag{2.6}$$

2.2. Gravitational sphere of influence

Since every particle in our Kepler system has a mass, they all influence each other through the gravitational force. However, due to the gravitational force applied by the large central mass that all planets orbit, the gravitational force between non-central particles is often negligible. We are interested in the case where the force between non-central planets is **not** negligible. For this we will use the Laplace sphere of influence, defined as: *The radius of a spherical region where the perturbing effect of the Sun on the particle's planetocentric orbit is lower than the perturbing effect of the planet on the particle's heliocentric orbit* [3]. When a particle enters said sphere of influence, the interplanetary gravitational force is stronger than the force between the particle and the central mass. In this scenario, we perform a scattering event within the CM-frame of the planet and the particle. During this scattering event the gravitational force of the Sun is **not** neglected. The same assumptions required to derive the Laplace sphere of influence will be applied to the Center-of-Mass (CM) frame to show that the gravitational force of the Sun is indeed negligible during the scattering event.

We shall now derive the expression for the Laplace sphere of influence of a planet. To start off, consider a 3-body problem with a Sun, a planet and a satellite (see Figure 2.2). The Laplace sphere of the planet is then the region in space in which we consider the planet to be the central body that the satellite is orbiting, instead of the Sun.

We start by considering the equations of motion for the satellite in the reference frame of the Sun and of a planet. For the planetary frame, we consider the planet with mass m to be the main mass dictating the attraction with a perturbation caused by the Sun $M_\odot$. The equation of motion for the satellite therefore is [2]:

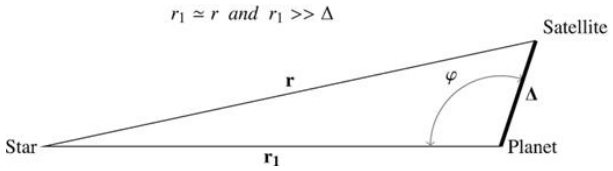

Figure 2.2: Geometry of the three-body problem (not to scale). $\mathbf{r_1}$ and $\mathbf{r}$ are the heliocentric position vectors of the planet and the satellite, respectively. In the reference frame attached to the planet, the position vector of the satellite is $\Delta = \mathbf{r} - \mathbf{r_1}$ [3]

$$\ddot{\boldsymbol{\Delta}} = -\frac{Gm}{\Delta^3}\boldsymbol{\Delta} - GM_\odot\left[\frac{\boldsymbol{r}}{r^3} - \frac{\boldsymbol{r}_1}{r_1^3}\right] = \boldsymbol{A}_1 + \boldsymbol{F}_1 \tag{2.7}$$

Here, $\boldsymbol{\Delta} = \boldsymbol{r} - \boldsymbol{r_1}$. $\boldsymbol{A_1}$ is the central acceleration of the satellite caused by the Planet and $\boldsymbol{F}_1$ is the perturbation caused by the Sun. For intuition's sake, this force $\boldsymbol{F}_1$ is the tidal interaction between the Sun and the Satellite which causes slight perturbations in the Satellite's orbit.

$$\begin{cases} \boldsymbol{A}_1 = -\dfrac{Gm}{\Delta^3}\boldsymbol{\Delta}, & A_1 = \frac{Gm}{\Delta^2}, \\ \boldsymbol{F}_1 = -GM_\odot\left[\dfrac{\boldsymbol{r}}{r^3} - \dfrac{\boldsymbol{r}_1}{r_1^3}\right], & F_1 \simeq \frac{GM_\odot\Delta}{r_1^3}\sqrt{1+3\cos^2\phi}, \end{cases} \tag{2.8}$$

Now for the heliocentric frame, we see that for the equation of motion, acceleration and magnitude we have the following set of equations:

$$\ddot{\boldsymbol{r}} = -\frac{GM_\odot}{r^3}\boldsymbol{r} - Gm\left[\frac{\boldsymbol{\Delta}}{\Delta^3} + \frac{\boldsymbol{r}_1}{r_1^3}\right] = \boldsymbol{A} + \boldsymbol{F} \tag{2.9}$$

$$\begin{cases} \boldsymbol{A} = -\dfrac{GM_\odot}{r^3}\boldsymbol{r}, & A = \frac{GM_\odot}{r^2} \simeq \frac{GM_\odot}{r_1^2}, \\ \boldsymbol{F} = -Gm\left[\dfrac{\boldsymbol{\Delta}}{\Delta^3} + \dfrac{\boldsymbol{r}_1}{r_1^3}\right], & F \simeq \frac{Gm}{\Delta^2}, \end{cases} \tag{2.10}$$

Following the same logic, $\boldsymbol{A}$ is the central acceleration of the satellite caused by the Sun, and $\boldsymbol{F}_1$ is the tidal interaction caused by the Planet.

In equation 2.8, $\cos\phi = \frac{\boldsymbol{r}_1\cdot\boldsymbol{\Delta}}{r_1\Delta}$. F and F_1 are derived by writing $\left\|\frac{\boldsymbol{\Delta}}{\Delta^3} + \frac{\boldsymbol{r}_1}{r_1^3}\right\|$ and $\left\|\frac{\boldsymbol{r}}{r^3} - \frac{\boldsymbol{r}_1}{r_1^3}\right\|$ as functions of $u = \frac{\Delta}{r_1}$ and $\cos\phi$. Since u can be considered small, we truncate the expressions to the 0^{th} order in u. The full derivation of the magnitudes of $\boldsymbol{F}$ and $\boldsymbol{F}_1$ is extensive and can be found in the paper by Chebotarev [4]. To obtain the naturally bounding surface of the sphere of influence, we equate the ratio of Solar accelerations to the ratio of Planetary accelerations:

$$\frac{A}{F} = \frac{A_1}{F_1} \tag{2.11}$$

The sphere of influence is then the area where $\frac{A_1}{F_1} > \frac{A}{F}$ holds. Intuitively, we are looking for the surface in space where the gravitational force exerted by the Planet on the Satellite is larger than the gravitational force exerted by the Sun on the Satellite. This will give us a volume space in which the gravitational force of the Planet on the Satellite becomes significant enough to account for in gravitational interactions. Substituting equations 2.10 and 2.8 into 2.11 now gives us:

$$s^{\text{inf}} = r_1\left(\frac{m^2}{M_\odot^2}\right)^{1/5}\frac{1}{(1+3\cos^2\phi)^{1/10}} \tag{2.12}$$

Now since $1 \le (1+3\cos^2\phi)^{1/10} \le 2^{1/5} \simeq 1.15$, we approximate this value by 1. This now results in the final expression for the Laplace sphere of influence:

$$s^{\text{inf}} = r_1 \left(\frac{m}{M_\odot} \right)^{2/5} \tag{2.13}$$

2.3. Elastic collisions using hyperbolic orbit

In a later section we will show that during the encounter, the gravitational force of the Sun is actually not completely neglected in the following derivation, but that the gravitational force of the Sun cancels out for the relative coordinate $\boldsymbol{u}$ between the colliding planets if approximated by a homogeneous field. Thus we shall only include the gravitational force between the respective planets. The problem then simplifies to a classical two-body problem. Since the planets do not collide in this case, energy is conserved and we can model this scenario as an elastic collision. The planets will be tracing a hyperbolic trajectory during the collision, as can be seen in figure 2.3.

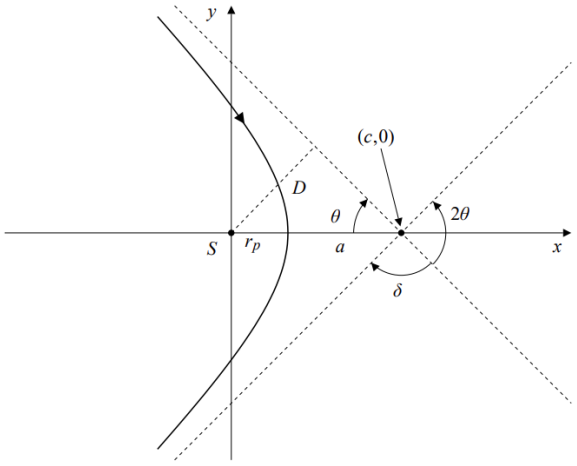

Figure 2.3: Hyperbolic trajectory of a close encounter with the large central mass and asymptotes of the relative coordinate. In this figure, S is the central mass. D is the shortest distance of the incoming asymptote to the origin, a is the semi-transverse axis, c is the semi-focal separation, r_p is the distance between the trajectory and the central mass at periapsis ($y = 0$), θ is the angle between the x-axis and the incoming asymptote and δ is the angle through which the relative coordinate's path is deflected by the gravitational attraction of the central mass [9]

Consider two particles m_1 and m_2 moving on elliptical orbits, with position vectors $\boldsymbol{r}_1$ and $\boldsymbol{r}_2$ and velocity vectors $\boldsymbol{v}_1$ and $\boldsymbol{v}_2$ respectively. The interaction between the particles can be described by the relative coordinate $\boldsymbol{d} = \boldsymbol{r}_2 - \boldsymbol{r}_1$. The relative coordinate moves in a hyperbolic orbit with velocity $\boldsymbol{u} = \boldsymbol{v}_2 - \boldsymbol{v}_1$ in the center-of-mass frame [11]. The trajectory of the relative coordinate will be approximated using its asymptotes. Before the scattering event, the relative coordinate moves on a straight line $\boldsymbol{d}_i(t)$ with constant velocity $\boldsymbol{u}_1$. By conservation of momentum, we immediately find that the magnitude of the velocity vector is conserved, hence $u_f = u_i = u$. The shortest distance between the two masses is reached when $\boldsymbol{d}_i \perp \boldsymbol{u}_i$, and we define $\boldsymbol{d}_i^\perp$ for the position vector where this is the case (equal to the dashed line with length D in 2.3). At this point, the scattering event gets executed by rotating the direction of the position and velocity both by an angle $\delta = \pi - 2\theta$. The particle then continues its trajectory with velocity $\boldsymbol{u}_f$, starting from $\boldsymbol{d}_f^\perp$, which is similarly defined as the position vector where $\boldsymbol{d}_f \perp \boldsymbol{u}_f$. By conservation of angular momentum, $\boldsymbol{d}_i \perp \boldsymbol{u}_i \times \boldsymbol{d}_f \perp \boldsymbol{u}_f$. Hence $d_f^\perp = d_i^\perp = d^\perp$.

From the geometry of Figure 2.4, we see that $\tan\theta = \frac{b}{a}$. Since $\theta = \frac{\pi}{2} - \frac{\delta}{2}$ and $\tan\left(\frac{\pi}{2} - \frac{\delta}{2}\right) = \left(\tan\frac{\delta}{2}\right)^{-1}$, it follows that $\delta = 2\arctan\frac{a}{b}$. Letting $d = |\boldsymbol{d}|$, the conservation of energy equation for a hyperbolic Keplerian orbit is given by the *vis-visa equation* (where a is defined to be positive) [8].

$$u^2 = G(m_1 + m_2)\left(\frac{2}{d} + \frac{1}{a}\right) \tag{2.14}$$

When $d \to \infty$, we find that $a = \frac{G(m_1+m_2)}{u^2}$. Since $c^2 = a^2 + b^2$, we find two angle-angle-side $\left(\frac{pi}{2}, \theta, c\right)$ congruent triangles from which it follows that $b = D$. From the geometry of Figure 2.4 it follows that D is equal to the

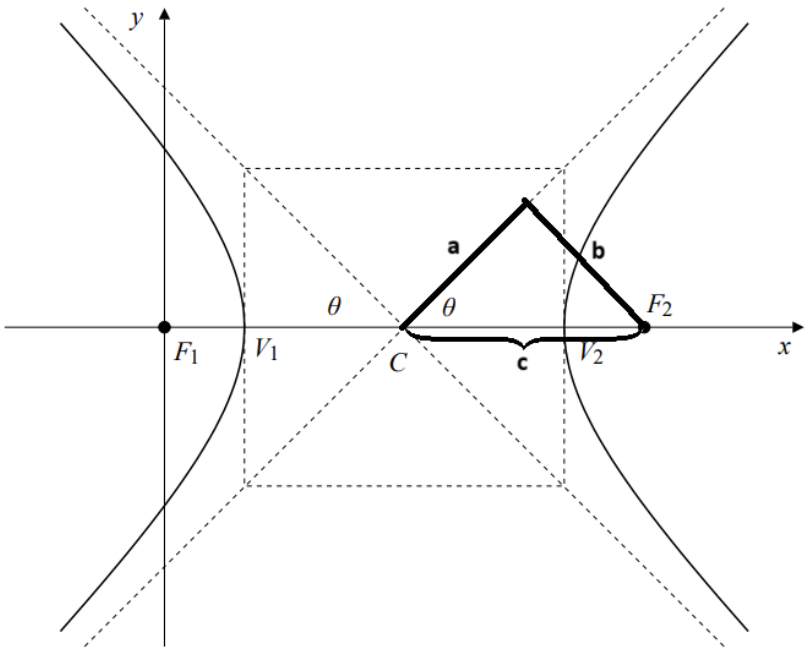

Figure 2.4: Geometry of a hyperbola. In this figure, a is the semi-transverse axis, b is the semi-conjugate axis, $c = \sqrt{a^2 + b^2}$ is the semi-focal separation, θ is the angle between the x-axis and the incoming asymptote. F_1 and F_2 are the focal points with vertices V_1 and V_2 respectively. $C = (c, 0)$ is the centre of the hyperbole. [1]

shortest distance of the incoming asymptote to the origin, which is the length $d^\perp$ of the vector $\boldsymbol{d}_i^\perp$ that is perpendicular to $\boldsymbol{u}_i$. Hence $b = d^\perp$. We can now compute the rotation by using:

$$\begin{bmatrix} \boldsymbol{d}_f^\perp \\ \boldsymbol{u}_f \end{bmatrix} = \mathscr{R}_\delta \begin{bmatrix} \boldsymbol{d}_i^\perp \\ \boldsymbol{u}_i^\perp \end{bmatrix} \tag{2.15}$$

where

$$\mathscr{R} = \begin{bmatrix} \cos\delta & \frac{b}{u}\sin\delta \\ -\frac{u}{b}\sin\delta & \cos\delta \end{bmatrix} = \begin{bmatrix} \frac{b^2-a^2}{c^2} & \frac{2ab^2}{\mu c^2} \\ -\frac{2au}{c^2} & \frac{b^2-a^2}{c^2} \end{bmatrix} \tag{2.16}$$

The placement of the plus or minus signs on the off-diagonal elements follows from the fact that the force acting on the relative coordinate is attractive.

2.4. Direct inelastic collisions between bodies

It is also possible for two particles i and j to directly collide and merge with each other (we assume the planets do not fragment). In this case, kinetic energy is not always conserved, with the remaining energy for example resulting in heat or sound. However, (angular) momentum is conserved. Using these laws of conservation, the orbit of the newly formed planet can be determined. Here, s is the radius of the particle, m is its mass, $\boldsymbol{r}$ the position vector, $\boldsymbol{v}$ is the momentum, $\boldsymbol{L}$ is the angular momentum, ℓ is the semi-latus rectum of the orbit, r is

the radial distance, $\boldsymbol{\epsilon}$ is the eccentricity vector and ϵ is the total eccentricity:

$$s_{new} = \sqrt[3]{s_i^3 + s_j^3}, \tag{2.17}$$

$$m_{new} = m_i + m_j \tag{2.18}$$

$$\boldsymbol{r}_{new} = \frac{m_i \boldsymbol{r}_i + m_j \boldsymbol{r}_j}{m_{new}} \tag{2.19}$$

$$\boldsymbol{v}_{new} = \frac{m_i \boldsymbol{v}_i + m_j \boldsymbol{v}_j}{m_{new}} \tag{2.20}$$

$$\boldsymbol{L}_{new} = \boldsymbol{L}_i + \boldsymbol{L}_j \tag{2.21}$$

$$\ell_{new} = \frac{\boldsymbol{L}_{new} \cdot \boldsymbol{L}_{new}}{GMm^2} \tag{2.22}$$

$$r_{new} = \sqrt{\boldsymbol{r}_{new} \cdot \boldsymbol{r}_{new}} \tag{2.23}$$

$$\boldsymbol{\epsilon}_{new} = \frac{\boldsymbol{v}_{new} \times \boldsymbol{L}_{new}}{GMm_{new}} - \frac{\boldsymbol{r}_{new}}{r_{new}} \tag{2.24}$$

$$\epsilon_{new} = \sqrt{\boldsymbol{\epsilon} \cdot \boldsymbol{\epsilon}} \tag{2.25}$$

2.5. Effect of the Sun's gravitational pull during close encounter

We further continue using the situation described in Section 2.2. Suppose the Satellite and Planet are such that they are within each other's spheres of influence and that the assumptions made in 2.2 hold ($r \simeq r_1$ and $r_1 \gg \Delta$). Let the mass of the Planet be m_1, Satellite be m_2 and Star be $M_\odot$. The equations of motion for m_1 and m_2 are as follows:

$$\begin{aligned} \boldsymbol{a}_1 &= -\tfrac{GM_\odot}{r_1^2}\hat{\boldsymbol{r}}_1 + \tfrac{Gm_2}{\Delta^2}\hat{\boldsymbol{\Delta}} \\ \boldsymbol{a}_2 &= -\tfrac{GM_\odot}{r^2}\hat{\boldsymbol{r}} - \tfrac{Gm_1}{\Delta^2}\hat{\boldsymbol{\Delta}} \end{aligned} \tag{2.26}$$

Here the first term in 2.26 represents the gravitational acceleration exerted on the planet by the central mass M. To now obtain the equation of motion for the relative coordinate $\boldsymbol{u} = \boldsymbol{v}_2 - \boldsymbol{v}_1$ in the center-of-mass frame, we subtract the top equation from the bottom equation. This gives us:

$$\boldsymbol{a}_2 - \boldsymbol{a}_1 = -GM\left(\frac{1}{r^2}\hat{\boldsymbol{r}} - \frac{1}{r_1^2}\hat{\boldsymbol{r}}_1\right) - \frac{G}{\Delta^2}(m_2 + m_1)\hat{\boldsymbol{\Delta}} \tag{2.27}$$

Since we use the same assumptions made in 2.2, namely that $r \simeq r_1$ and $r_1 \gg \Delta$, we can further simplify equation 2.27. The term $\left|\frac{1}{r^2}\hat{\boldsymbol{r}} - \frac{1}{r_1^2}\hat{\boldsymbol{r}}_1\right| \approx 0$ as we apply $r \simeq r_1$, leaving us with:

$$\boldsymbol{a}_2 - \boldsymbol{a}_1 = -\frac{G}{\Delta^2}(m_2 + m_1)\hat{\boldsymbol{\Delta}} + \mathcal{O}\left(\frac{1}{r^3}\right) \tag{2.28}$$

We see here that the term representing the gravitational force of the central mass $M_\odot$ on the planets has been canceled. Since the relative coordinate $\boldsymbol{u} = \boldsymbol{v}_2 - \boldsymbol{v}_1$ is just an integrated version of equation 2.28, we see that the equation of motion simplifies to a situation without the central mass $M_\odot$ exerting any force on the relative coordinate $\boldsymbol{u}$. This means that our assumption made in section 2.3 is justified, seeing as we are not actually "pretending" the Sun does not exist during the elastic collision, but merely that its influence on the elastic collision is negligible.

2.6. Initial state: a flat circular disk

To accurately simulate an N-body Kepler system, we require realistic distributions for certain physical parameters. In the simulation, every particle has a mass $m_i \in [m_{\min}, m_{\max}]$, semi-major axis $a_i \in [a_{\min}, a_{\max}]$

an inclination $I_i \in [0, I_{\max}]$ and eccentricity $\epsilon_i \in [0, \epsilon_{\max}]$. The volume in which all the particles exist is given by:

$$V = \int_0^{2\pi} \int_{\pi/2-I_{\max}}^{\pi/2+I_{\max}} \int_{a_{\min}}^{a_{\max}} r^2 \sin\theta \, dr \, d\theta \, d\phi = \frac{4\pi}{3}(a_{\max}^3 - a_{\min}^3) \sin I_{\max} \tag{2.29}$$

For the distribution of the radii s of the particles, we take $dN/dS \propto s^{-3}$, which is about equal to the distribution of an asteroid belt [5]. Assuming that every particle has the same density of mass, we have that $m \propto s^3$ and therefore $dN/dm \propto m^{-5/3}$. To determine the probability distribution of the particle mass $p(m)$, we must have that $\int_{m_{\min}}^{m_{\max}} p(m)dm = \int_{m_{\min}}^{m_{\max}} Am^{-5/3}dm = 1$. From this, it follows that:

$$p(m) = \frac{2}{3} \frac{(m_{\max} m_{\min})^{2/3}}{m_{\max}^{2/3} - m_{\min}^{2/3}} m^{-5/3} \tag{2.30}$$

To ensure that the system has a uniform particle density for its entire volume, we require that $dN/da \propto a^2$ and $dN/dI \propto \sin I$. Since $\int_{a_{\min}}^{a_{\max}} p(a)da = \int_{a_{\min}}^{a_{\max}} Ba^2 da = 1$, we have that:

$$n(a) = \frac{3}{a_{\max}^3 - a_{\min}^3} a^2 \tag{2.31}$$

Then for the inclination it follows from $\int_0^{I_{\max}} p(I)dI = \int_0^{I_{\max}} C \sin I dI = 1$ that:

$$p(I) = \frac{1}{1 - \cos I_{\max}} \sin I \tag{2.32}$$

The eccentricity is drawn from a uniform distribution $\mathcal{U}[0, \epsilon_{\max}]$, and therefore $p(\epsilon)$ has a constant value in this interval. In Figure 4.2 the theoretical distributions with values given in Table 3.2 and $\epsilon_{\max} = 0.1$ are shown with orange dotted lines. To more clearly visualize the nature of the distribution of objects, Figure 2.5 shows a top-down view of the planets in their initial state.

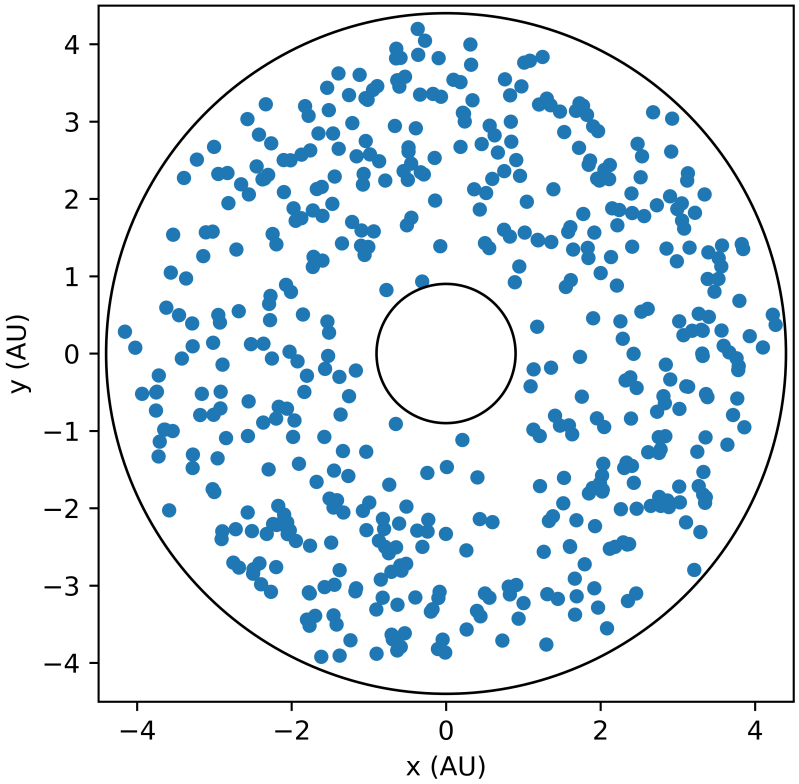

Figure 2.5: Top-down scatterplot of the planets in the initial state of a simulation with values given in Table 3.2 and $\epsilon_{\max} = 0.1$. The inner black circle has a radius $r_{\min} = a_{\min}(1-\epsilon_{\max})$, whereas the outer black circle has a radius $r_{\max} = a_{\max}(1+\epsilon_{\max})$. All planets fall neatly between these inner and outer circles.

3

Simulation Method

In this chapter we will completely describe the algorithm used to predict, execute and appropriately handle both close encounters, direct collisions and particle ejections due to particle interactions. This will further build upon Visser's algorithm [11], Jort Koks' close encounters [9] and Moorlag's direct collisions [6]. The system is initialized in the same way as in the research paper by Jort Koks [9], after which the main loop of Visser's algorithm [11] will be described which the system uses to evolve in time. At last, the separate cases of close encounters and direct collisions between particles will be elaborated. These cases include the handling of possible ejection of particles from the system.

3.1. Initialization

As mentioned before, the initialization process is the exact same as the paper by Jort Koks [9], and therefore this paper will not go into much detail regarding said process. In short, we number every particle $i = 1, \ldots, N$. For every particle, we store the following set of variables:

$$\{t_i^0, a_i, c_i, s_i, m_i, \boldsymbol{r}_i^0, \boldsymbol{L}_i, \boldsymbol{\epsilon}_i, \omega_i, \boldsymbol{v}_i^0\} \tag{3.1}$$

These variables are determined by choosing the six orbital parameters $a_i, \epsilon_i, I_i, \bar{\omega}, \Omega_i$ and M_i such that they form a uniform particle disk. The exact processes and distributions used are described by Jort Koks [9].

Parameter	Domain
m_i	$m_{\min}[1-\xi(1-(m_{\min}/m_{\max}^{2/3}]^{-}3/2$
a_i	$\sqrt[3]{a_{\min}^3 + \xi\left(a_{\max}^3 - a_{\min}^3\right)}$
ϵ_i	$\epsilon_{\max}\xi$
I_i	$\arccos\left(\cos I_{\max} + \xi\left(1 - \cos I_{\max}\right)\right)$
$\overline{\omega}$	$2\pi\xi$
Ω_i	$2\pi\xi$
M_i	$2\pi\xi$

Table 3.1: Initialization domains of the particles in the system. We let $\xi \sim \mathcal{U}[0,1]$ randomly for the parameters of each particle. See Jort Koks [9] for derivations of the shown expressions.

Parameter	Standard value	Test domain
N	500	
$m_{\max}$	10^{-7} $M_\odot$	
$m_{\min}$	10^{-10} $M_\odot$	
$a_{\max}$	4 AU	
$a_{\min}$	1 AU	
$\epsilon_{\max}$	0.1	{0.1, 0.2, 0.4}
$I_{\max}$	0.1	

Table 3.2: Boundaries of the initialization domains. The values of each of the parameters are picked within the set of their test domains, while keeping all other parameters fixed at their standard value.

3.2. Main loop of the algorithm

The general algorithm used in the simulation is described in Visser's paper [11]. This time the algorithm includes both direct collisions and close encounters between particles. The case of particle ejection due to interactions is also appropriately handled.

1. If the scattering list is empty, end the simulation.
2. Take the pair (i, j) with the soonest scattering, that being the first scattering in the list. If the time to wait for this scattering event is longer than $0.2 \cdot 10^6$ y, end the simulation. Else, perform the scattering event, differentiating between a direct collision or close encounter.
3. Update the time t to the time $t^1_{(i,j)}$ of the scattering.
4. Remove any pair containing i and any pair containing j from the list of scattering pairs.
5. Remove the particles i and j from the particle list.
6. Check if the orbit(s) of the new particle(s) intersect the central mass or are ejected:
   (a) If the interaction is a direct collision where the new planet intersects the central mass or is ejected, go to the next scattering on the list. (no particle is added)
   (b) If the interaction is a close encounter where both separate planets either intersect the central mass or get ejected, go to the next scattering on the list. (no particle is added)
7. For the retained particles, create new particles i' and/or j' (in case of a close encounter with both particles conserved) defined by $\{t^1_i, a_i, c_i, s_i, m_i, \boldsymbol{r_i}^0, \boldsymbol{L_i}, \boldsymbol{\epsilon}_i, \omega_i, \boldsymbol{v}^0_i\}$ and/or $\left\{t^1_j, a_j, c_j, s_j, m_j, \boldsymbol{r}^0_j, \boldsymbol{L}_j, \boldsymbol{\epsilon}_j, \omega_j, \boldsymbol{v}^0_j\right\}$.
8. For any new particle, consider the other particles and determine the new scatterings caused by adding new particle(s) to the system. Determine the time of these scatterings.
9. Merge the times of the new scatterings with the pre-existing scattering time list (with scatterings involving i and j now removed).
10. Sort the merged list of scattering times, the soonest scattering event being first. Also add the new particles i' and/or j' to the list of all particles.

3.3. Scattering Detection

To obtain the list of scatterings used in the main algorithm, we first have to detect these scattering pairs and then sort them by the time at which they occur. The methods described for detecting these scattering events are based on results from [11].

3.3.1. Determining scattering pairs

For a particle i, we first determine the gravitational sphere of influence $s_i^{\text{inf}} = a_i \left(\frac{m_i}{M}\right)^{2/5}$. The interval of interaction for a particle ranges from periapsis to apoapsis: $[a_i - c_i - s_i^{\text{inf}}, a_i + c_i + s_i^{\text{infz}}]$. For an encounter to even be possible with a particle j, we must have that the intervals of i and j overlap such that $a_i + c_i + s_i^{\text{inf}} \geq a_j - c_j - s_j^{\text{inf}}$. Suppose we found a pair $(i, j) = (1, 2)$ with $a_1 > a_2$ which meets the following criteria. We then compute the

direction of the nodal line $\boldsymbol{K}$ and its magnitude K:

$$\boldsymbol{K} = \boldsymbol{L}_1 \times \boldsymbol{L}_2, \quad K = \sqrt{\boldsymbol{K} \cdot \boldsymbol{K}} \tag{3.2}$$

For the particles (1,2) we then further compute the semi-latus rectum ℓ, the two intersection points with the nodal line $\boldsymbol{r}_\pm$ and the velocities $\boldsymbol{v}_\pm$ at these points:

$$\ell_1 = \frac{\boldsymbol{L}_1 \cdot \boldsymbol{L}_1}{GMm_1^2}, \quad \ell_2 = \frac{\boldsymbol{L}_2 \cdot \boldsymbol{L}_2}{GMm_1^2} \tag{3.3}$$

$$\boldsymbol{r}_{1,\pm} = \frac{\boldsymbol{K}\ell_1}{\pm K + \boldsymbol{\epsilon}_1 \cdot \boldsymbol{K}}, \quad \boldsymbol{r}_{2,\pm} = \frac{\boldsymbol{K}\ell_2}{\pm K + \boldsymbol{\epsilon}_2 \cdot \boldsymbol{K}} \tag{3.4}$$

$$r_{1,\pm} = \sqrt{\boldsymbol{r}_{1,\pm} \cdot \boldsymbol{r}_{1,\pm}}, \quad r_{2,\pm} = \sqrt{\boldsymbol{r}_{2,\pm} \cdot \boldsymbol{r}_{2,\pm}} \tag{3.5}$$

$$\boldsymbol{v}_{1,\pm} = \frac{\boldsymbol{L}_1}{m_1\ell_1} \times \left(\boldsymbol{\epsilon_1} + \frac{\boldsymbol{r}_{1,\pm}}{r_{1,\pm}}\right), \quad \boldsymbol{v}_{2,\pm} = \frac{\boldsymbol{L}_2}{m_2\ell_2} \times \left(\boldsymbol{\epsilon_2} + \frac{\boldsymbol{r}_{2,\pm}}{r_{2,\pm}}\right) \tag{3.6}$$

To then determine the minimal orbit intersection distance (MOID), we consider the tangent lines of the orbits at the points $\boldsymbol{r}_{1,\pm}$ and $\boldsymbol{r}_{2,\pm}$. The minimal distance $\boldsymbol{r}_{1,\pm}^{\min}$ and $\boldsymbol{r}_{1,\pm}^{\min}$ between these lines can then be found. The positions can be written as:

$$\boldsymbol{r}_{1,\pm}^{\min} = \boldsymbol{r}_{1,\pm} + \left[(\boldsymbol{r}_{2,\pm} - \boldsymbol{r}_{1,\pm}) \cdot \frac{\boldsymbol{v}_{2,\pm} \times (\boldsymbol{v}_{1,\pm} \times \boldsymbol{v}_{2,\pm})}{\left|\boldsymbol{v}_{1,\pm} \times \boldsymbol{v}_{2,\pm}\right|^2}\right] \boldsymbol{v}_{1,\pm} \tag{3.7}$$

$$\boldsymbol{r}_{2,\pm}^{\min} = \boldsymbol{r}_{2,\pm} + \left[(\boldsymbol{r}_{2,\pm} - \boldsymbol{r}_{1,\pm}) \cdot \frac{\boldsymbol{v}_{1,\pm} \times (\boldsymbol{v}_{1,\pm} \times \boldsymbol{v}_{2,\pm})}{\left|\boldsymbol{v}_{1,\pm} \times \boldsymbol{v}_{2,\pm}\right|^2}\right] \boldsymbol{v}_{2,\pm} \tag{3.8}$$

The shortest distance between the two lines is then:

$$d_\pm^{\min} = |\boldsymbol{r}_{2,\pm}^{\min} - \boldsymbol{r}_{1,\pm}^{\min}| = \left|(\boldsymbol{r}_{2,\pm} - \boldsymbol{r}_{1,\pm}) \cdot \frac{(\boldsymbol{v}_{1,\pm} \times \boldsymbol{v}_{2,\pm})}{\left|\boldsymbol{v}_{1,\pm} \times \boldsymbol{v}_{2,\pm}\right|}\right| \tag{3.9}$$

In the case of $d_\pm^{\min} \leq max\{s_1, s_2\}$, we perform a direct collision scattering. Else, if $d_\pm^{\min} \leq max\{s_1^{\inf}, s_2^{\inf}\}$, we perform a close encounter.

3.3.2. Calculating the time of a scattering

Suppose we have two particles $(i, j) = (1,2)$ such that either expression above holds. To calculate the time at which any scattering occurs (both collision and close encounter), we first need to know the time for which the particles first cross the nodal line $\boldsymbol{K}$. Let these times be t_1^1 and t_2^1 respectively. For every set of particles, we only need to know the difference in eccentric anomaly $\Delta E = E^1 - E^0$ between the position vectors $\boldsymbol{r}^1$ and $\boldsymbol{r}^0$. The angle ΔE can be written as the argument of a complex number as follows [11].

$$\Delta E = \arg\left[\left(\frac{\boldsymbol{r}^1}{a} - \frac{i r^1 \boldsymbol{v}^1}{a^2\omega}\right) \cdot \left(\frac{\boldsymbol{r}^0 - \boldsymbol{\epsilon}\boldsymbol{\epsilon} \cdot \boldsymbol{r}^0}{a - \epsilon^2 a} + \boldsymbol{\epsilon}\right) + \frac{\boldsymbol{r}^0 \cdot \boldsymbol{\epsilon}}{a} + \epsilon^2\right] \tag{3.10}$$

The scattering time $t_{k,l}$ is then the time where particles 1 and have completed an integer k and l number of orbits respectively after reaching their first intersection with the nodal line. This $t_{k,l}$ is computed by [11]:

$$t_{k,l} = kT + t^0 + \frac{\Delta E}{\omega} - \frac{\boldsymbol{\epsilon} \times (\boldsymbol{r}_1 - \boldsymbol{r}^0)}{\omega b} \cdot \frac{\boldsymbol{L}}{L} \tag{3.11}$$

where $0 \leq \Delta E < 2\pi$ due to it being the argument. The algorithm to determine the values of k and l is described in Chapter 6 of [11]. At the time $t_{k,l}$, we will then have our particles situated close enough to $\boldsymbol{r}_{1,\pm}^{\min}$ and $\boldsymbol{r}_{2,\pm}^{\min}$ to perform either a direct collision or close encounter.

3.4. Performing a close encounter event

In this section, step 2 of the main loop is elaborated upon. When planets get very close to each other, their gravitational pull can no longer be ignored and has to be accounted for. It is very computationally expensive to account for this gravitational pull dynamically, which is why planet trajectories are linearized. The process is divided into 3 phases: The period before the scattering event, the scattering event and the period after the scattering event.

3.4.1. Before scatter event

As was shown in equation 3.11, the scattering time can be calculated. The initial trajectory of the orbits of particles m_1 and m_2 is linearized around their respective positions $\boldsymbol{r}_1 = \boldsymbol{r}_1(t_{k,l})$ and $\boldsymbol{r}_2 = \boldsymbol{r}_2(t_{k,l})$ at the time $t_{k,l}$ ($\pm$ subscripts will be ignored in this section):

$$\boldsymbol{r}_{1,i}(t) = \boldsymbol{r}_1 + (t - t_{k,l})\boldsymbol{v}_{1,i}, \qquad \boldsymbol{r}_{2,i}(t) = \boldsymbol{r}_2 + (t - t_{k,l})\boldsymbol{v}_{2,i}, \tag{3.12}$$

$$\boldsymbol{v}_{1,i} = \boldsymbol{v}(\boldsymbol{r}_1), \qquad \boldsymbol{v}_{2,i} = \boldsymbol{v}(\boldsymbol{r}_2) \tag{3.13}$$

Here, $\boldsymbol{r}_1$ and $\boldsymbol{r}_2$ follow from equation 2.4 and $\boldsymbol{v}_{1,i}$ and $\boldsymbol{v}_{2,i}$ follow from equation 2.5. Since the scatter event theory is derived in a center-of-mass frame, we need to transform these coordinates. Before the scatter event, the relative mass $\mu = \frac{m1m2}{m1+m2}$ has initial position $\boldsymbol{d}_i$ and velocity $\boldsymbol{u}_i$:

$$\boldsymbol{d}_i(t) = \boldsymbol{r}_{2,i}(t) - \boldsymbol{r}_{1,i}(t), \qquad \boldsymbol{u}_i = \boldsymbol{v}_{2,i} - \boldsymbol{v}_{1,i} \tag{3.14}$$

The scatter event will be performed at the time $t^\perp$, when the distance from $\boldsymbol{d}_i(t)$ is minimized. This occurs when $\boldsymbol{d}_i(t) \cdot \boldsymbol{u}_i = 0$. Solving this equation for $t^\perp$ gives:

$$t^\perp = t_{k,l} - \frac{(\boldsymbol{r}_2 - \boldsymbol{r}_1) \cdot \boldsymbol{u}_i}{u^2} \tag{3.15}$$

which then gives us the position of the relative mass μ at this time $t^\perp$ as:

$$\boldsymbol{d}_i^\perp = \boldsymbol{d}_i(t^\perp) = \boldsymbol{r}_2 - \boldsymbol{r}_1 - \frac{(\boldsymbol{r}_2 - \boldsymbol{r}_1) \cdot \boldsymbol{u}_i}{u^2}\boldsymbol{u}_i \tag{3.16}$$

where the superscript is a result of the fact that $\boldsymbol{d}_i^\perp \perp \boldsymbol{u}_i$. Therefore $\left\{\frac{\boldsymbol{d}_i^\perp}{d}, \frac{\boldsymbol{u}_i}{u}\right\}$ forms an orthonormal basis in $\mathbb{R}^2$. The centre-of-mass $m_1 + m_2$ moves with position $\mathbf{R}_i(t)$ and velocity $\mathbf{V}_i$:

$$\mathbf{R}_i(t) = \frac{m_1\boldsymbol{r}_{1,i}(t) + m_2\boldsymbol{r}_{2,i}(t)}{m1 + m2}, \qquad \mathbf{R}_i(t) = \frac{m_1\boldsymbol{v}_{1,i} + m_2\boldsymbol{v}_{2,i}}{m1 + m2} \tag{3.17}$$

Since $\mathbf{R}_i(t)$ is constant, we can choose the inertial reference frame such that the CM is at rest in the origin and the total momentum is zero. This means that the particles m_1 and m_2 are moving, but with equal and opposite momenta. This situation then simplifies to the same situation as a single particle with mass equal to the reduced mass μ.

3.4.2. The scatter event

Since it is an ellastic collision, no energy loss takes place. The relative coordinate describes a hyperbolic orbit with parameters:

$$a = \frac{G(m_1 + m_2)}{u^2}, \quad b = d = |\boldsymbol{d}_i^\perp|, \quad c^2 = a^2 + b^2 \tag{3.18}$$

where $u = |\boldsymbol{u}_i| = |\boldsymbol{u}_f|$ due to conservation of momentum. The entering asymptote has direction $\boldsymbol{u}_i$ and the exiting asymptote has direction $\boldsymbol{u}_f$. Due to the gravitational scattering, a rotation of the position and velocity vector of the reduced mass μ of an angle $\delta = 2\arctan(a/b)$ occurs. From equations 2.15 and 2.16, we see that:

$$\boldsymbol{d}_f^\perp = \frac{b^2 - a^2}{c^2}\boldsymbol{d}_i^\perp + \frac{2ab^2}{uc^2}\boldsymbol{u}_i \tag{3.19}$$

$$\boldsymbol{u}_f = \frac{-2au}{c^2}\boldsymbol{d}_i^\perp + \frac{b^2 - a^2}{c^2}\boldsymbol{u}_i \tag{3.20}$$

3.4.3. After scatter event

The motion of the relative mass μ has now been set to velocity $\boldsymbol{u}_f$ and position $\boldsymbol{d}_f(t) = \boldsymbol{d}_f^{\perp} + (t - t^{\perp})\boldsymbol{u}_f$. Now the particles need to be transformed from the CM frame back to the particle coordinates $m_1 + m_2$ and $\mu = \frac{m_1 m_2}{m_1 + m_2}$. The equations for the velocities $\boldsymbol{v}_{1,f}$ and $\boldsymbol{v}_{2,f}$ after the scattering are:

$$\boldsymbol{v}_{1,f} = \boldsymbol{V}_i - \frac{m_2}{m_1 + m_2}\boldsymbol{u}_f, \qquad \boldsymbol{v}_{2,f} = \boldsymbol{V}_i - \frac{m_1}{m_1 + m_2}\boldsymbol{u}_f \tag{3.21}$$

The particles now travel along two straight lines given by:

$$\boldsymbol{r}_{1,f}(t) = \boldsymbol{R}_i(t) - \frac{m_2}{m_1 + m_2}\boldsymbol{d}_f(t) \tag{3.22}$$

$$\boldsymbol{r}_{2,f}(t) = \boldsymbol{R}_i(t) + \frac{m_1}{m_1 + m_2}\boldsymbol{d}_f(t) \tag{3.23}$$

Immediately after the scattering event, we see that:

$$\boldsymbol{r}_{1,f}(t^{\perp}) = \boldsymbol{R}^{\perp}{}_i(t) - \frac{m_2}{m_1 + m_2}\boldsymbol{d}_f^{\perp}(t) \tag{3.24}$$

$$\boldsymbol{r}_{2,f}^{\perp}(t) = \boldsymbol{R}_i(t^{\perp}) + \frac{m_1}{m_1 + m_2}\boldsymbol{d}_f^{\perp}(t) \tag{3.25}$$

3.5. Finding new scattering possibilities

After the scatter event, particles involved before the scatter event are removed. The new particles have their parameters as shown in equation 3.1 updated according to the following equations:

$$\boldsymbol{L} = m\boldsymbol{r} \times \boldsymbol{v}, \tag{3.26}$$

$$\ell = \frac{\boldsymbol{L} \cdot \boldsymbol{L}}{GMm^2}, \tag{3.27}$$

$$r = \sqrt{\boldsymbol{r} \cdot \boldsymbol{r}}, \tag{3.28}$$

$$\boldsymbol{\epsilon} = \frac{\boldsymbol{v} \times \boldsymbol{L}}{GMm} - \frac{\boldsymbol{r}}{r}, \tag{3.29}$$

$$\epsilon = \sqrt{\boldsymbol{\epsilon} \cdot \boldsymbol{\epsilon}} \tag{3.30}$$

The particle only stays in an elliptical orbit around the central mass and does not collide with it when $\epsilon < 1$ and $\ell > (1 + \epsilon)S$, where S is the radius of the central body. If these inequalities hold, then the particle stays in the system. Else it is ejected/destructed.

4

Results

In this chapter, the results are presented of 3 sets of 5 simulations. The maximum eccentricity $\epsilon_{\max} \in \{0.1, 0.2, 0.4\}$ is varied while keeping the other parameters as described in Table 3.2.

4.1. Maximum eccentricity of 0.1

In Figure 4.1, 5 simulations with $\epsilon_{\max} = 0.1$ are shown, plotting the total scatter count n_{scatt} versus the time t in years.

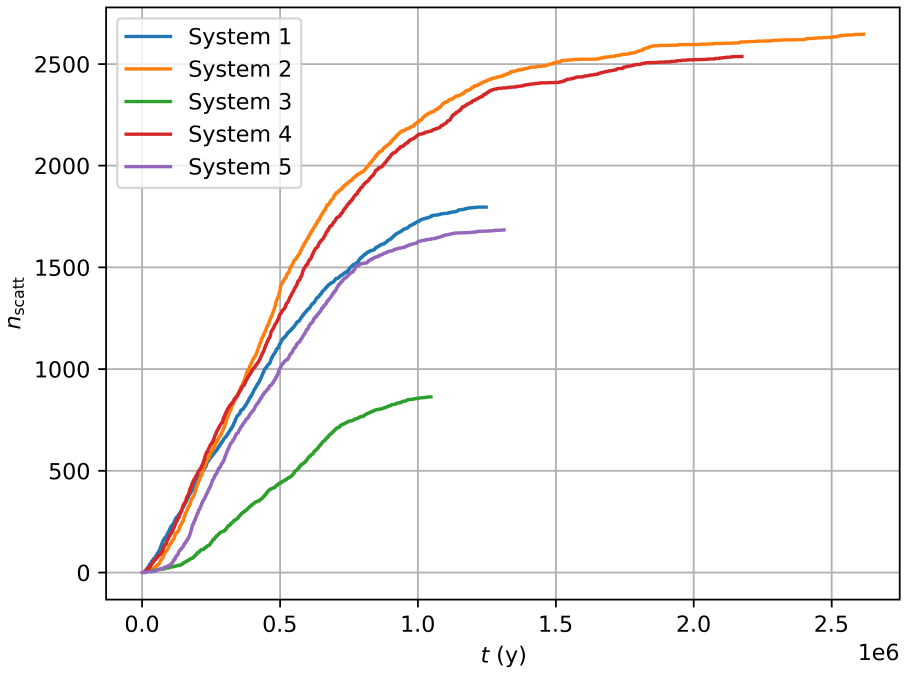

Figure 4.1: For five simulations with $\epsilon_{\max} = 0.1$, the total number of scatterings n_{scatt} is plotted versus the time t in years. Other relevant parameters are distributed as described in Table 3.1. The simulations stopped when the next scattering was more than 10^5y in the future

To further research the effects of many scatterings, we pick the system with the highest number of scatterings $n_{\max}$. In this case we will proceed using system 2 with $n_{\max} = 2647$. In Figure 4.2 the initial distributions of the parameters m, a, I and ϵ of the particles of system 2 are plotted with their theoretical distribution according to Table 3.1.

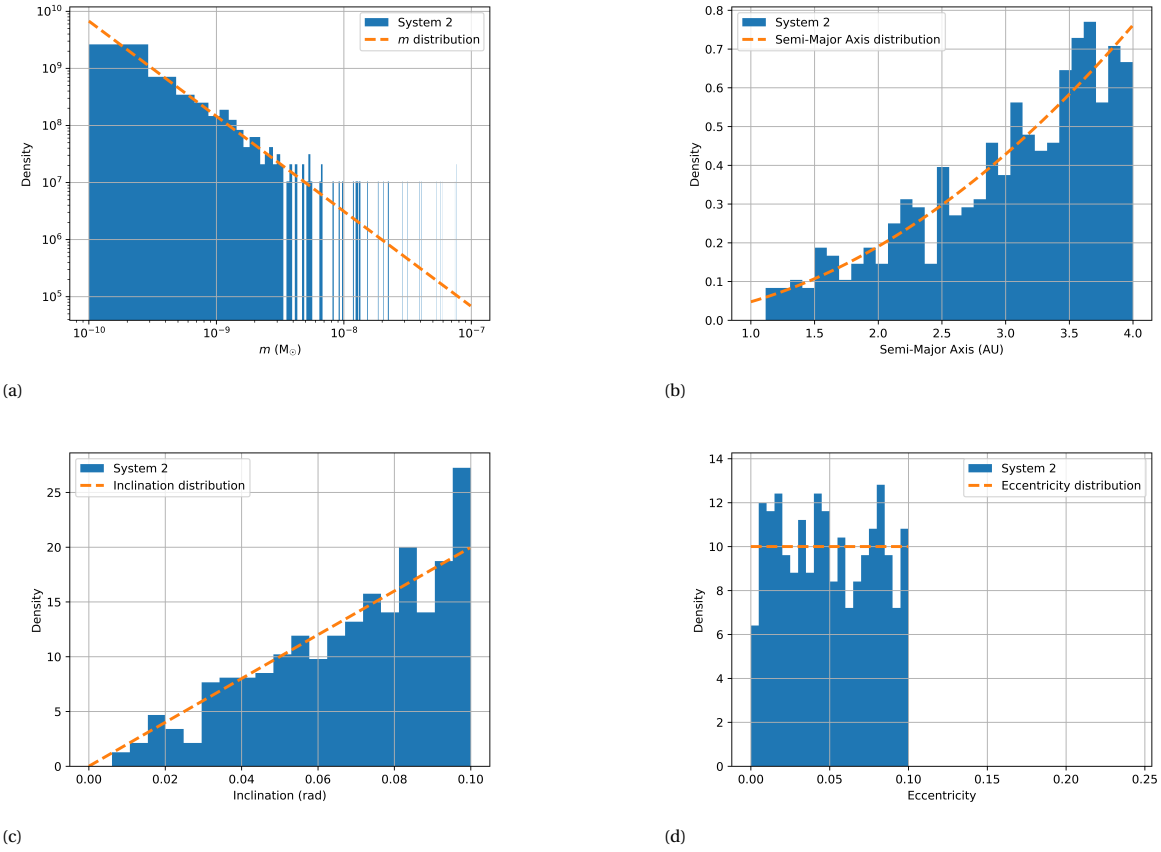

Figure 4.2: Density histograms showing the initial distributions of important parameters m, a, I and ϵ for system 2 for $\epsilon_{\max} = 0.1$. The orange lines indicate theoretical distributions from which the values for m_i, a_i, I_i and ϵ_i were generated for every particle $1 \leq i \leq 500$ using the formulas found in Table 3.1. (a): Density histogram log-log plot of the planetary masses m_i ($M_\odot$). (b) Density histogram plot of the Semi-Major Axis a_i (AU). (c) Density histogram plot of the Inclination I_i (rad). (d) Density histogram plot of the Eccentricity ϵ_i.

In order to showcase the effect of scatterings on the distribution of the eccentricity ϵ, the eccentricity distribution of the particles of system 2 is plotted at the start ($n_{\text{scatt}} = 0$) and at the end of the simulation ($n_{\text{scatt}} = n_{\text{max}}$). In Figure 4.3 we compare the eccentricity distribution in the initial and final state of system 2.

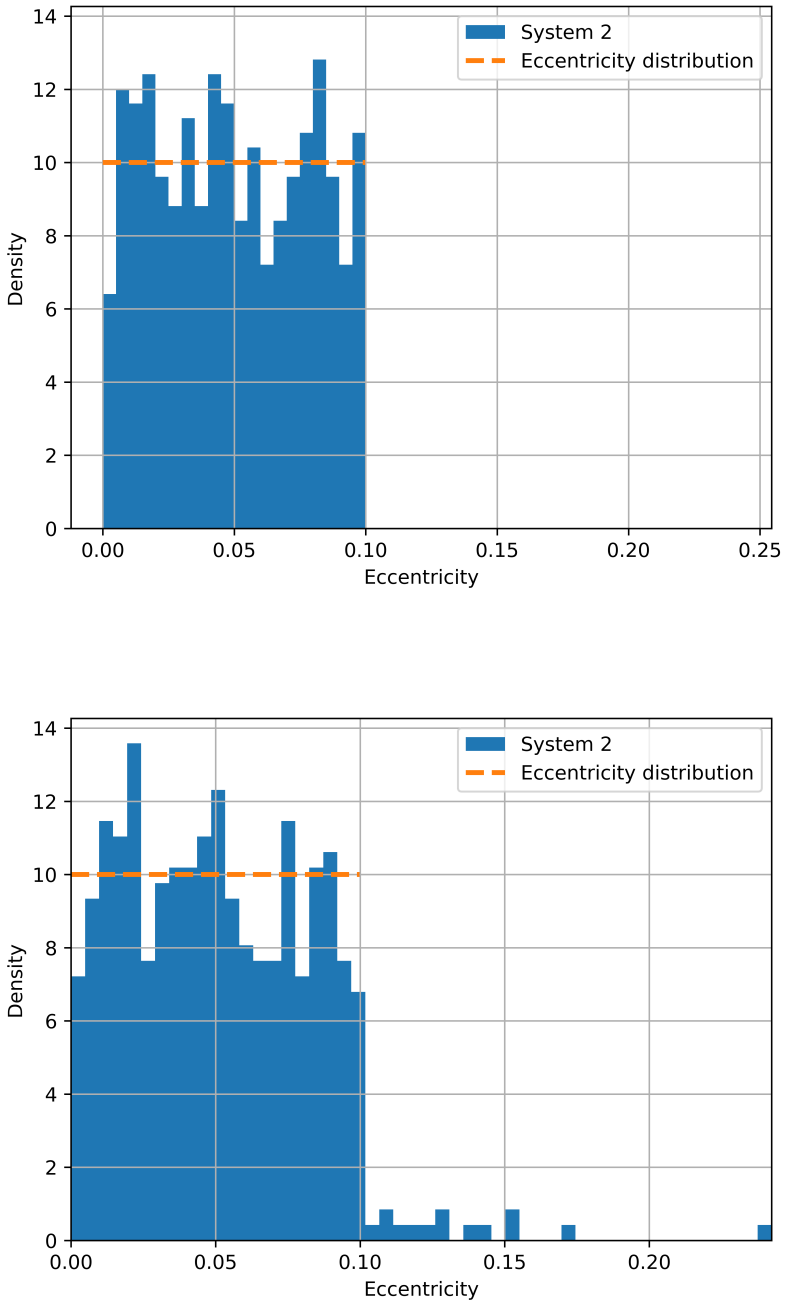

Figure 4.3: Above: Density histogram of the eccentricity of the initial particles in system 2. The orange line indicates the theoretical distribution used to generate ϵ_i found in Table 3.1. Below: Density histogram of the eccentricity of the final particles in system 2 at $n_{\text{scatt}} = n_{\text{max}} = 2647$ or after $t = 2.5$My. Here, the orange line of the initial eccentricity distribution is still drawn to more clearly showcase the change in distribution. Note that the total amount of planets is lower in the final state due to ejections.

To get an idea of the shape and distribution of the orbits of particles in system 2, both in the initial and final state, astronomy commonly uses (ϵ, a) plots. In Figure 4.4, we see scatter-plots of the particles of system 2 in both its initial and final state.

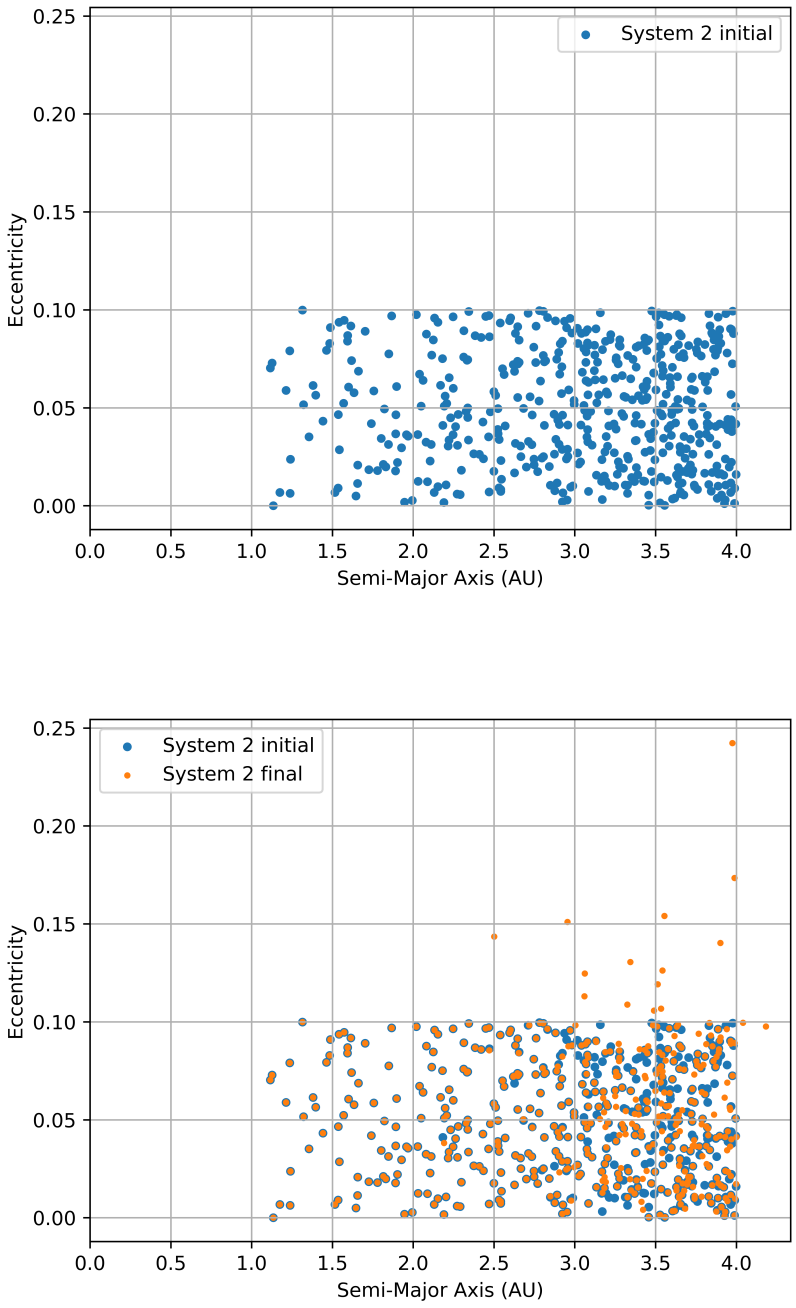

Figure 4.4: (ϵ, a) scatterplots of the particles in the disk. The minimum and maximum values of both ϵ and a can clearly be identified using the upper scatterplot by observing the box that all particles are contained by. This box is $[a_{\min}, a_{\max}] \times [\epsilon_{\min}, \epsilon_{\max}]$ as expected from the initial distribution parameters. Below: (ϵ, a) scatterplot of the particles in the final state of system 2 ($n_{\text{scatt}} = n_{\max} = 2647$). Note that the particles are no longer contained by the box $[a_{\min}, a_{\max}] \times [\epsilon_{\min}, \epsilon_{\max}]$. An orange dot on top of a blue dot means that that particle still has the same eccentricity and semi-major axis as in its initial state, indicating that it was not involved in any scattering events. We see that below 3AU, most particles have not been scattered, while above 3AU many particles have been scattered into high eccentric orbits.

As can be seen in the report made by Jort Koks [9], the simulations go through an initial phase where the scatter frequency is increasing. This is showcased for all systems in Figure 4.5.

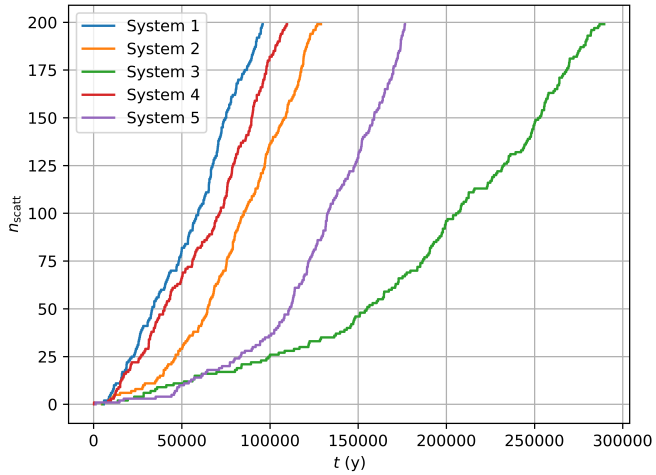

Figure 4.5: n_{scatt} plotted versus the time t in years for $n_{\text{scatt}} \leq 200$ for all systems with $\epsilon_{\text{max}} = 0.1$. $n_{\text{scatt}} = 200$ was chosen due to all simulated systems entering a phase of roughly constant scatter frequency after this scatter count. Some simulations take longer to enter this linear phase of the graph, while other systems start off almost linear already.

After $n_{\text{scatt}} = 200$, all systems go through a roughly linear period of growth. All systems exhibit a trend of decaying growth for $n_{\text{scatt}} \geq 200$, to which a curve can be fitted. The curve that most closely matches the shapes of the systems' (t, n_{scatt}) plots is $n_{\text{scatt}}(t) = n_{\text{max}} - ae^{-t/\tau}$. In Figure 4.6 the resulting curve-fit for system 2 can be found, fitted to values $200 \leq n_{\text{scatt}} \leq n_{\text{max}}$.

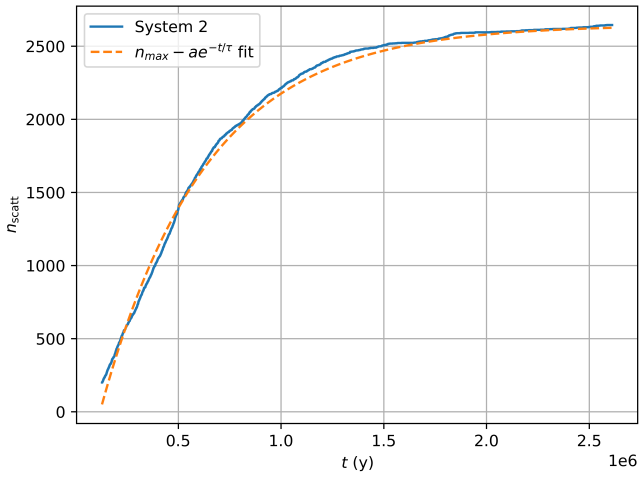

Figure 4.6: Number of scatterings of system 2 ($200 \leq n_{\text{scatt}} \leq n_{\text{max}} = 2647$) plotted versus the time t in years. The dashed orange line represents the results of a curve of shape $n_{\text{scatt}}(t) = n_{\text{max}} - ae^{-t/\tau}$ fitted to the data. n_{max} can only be determined after the simulation has been fully executed. The resulting fit parameters are $a = 3344 \pm 5$ and $\tau = (510 \pm 1) \cdot 10^3$y.

4.2. Maximum eccentricity of 0.2

In Figure 4.7, 5 simulations with $\epsilon_{\max} = 0.2$ are shown, plotting the total scatter count n_{scatt} versus the time t in years.

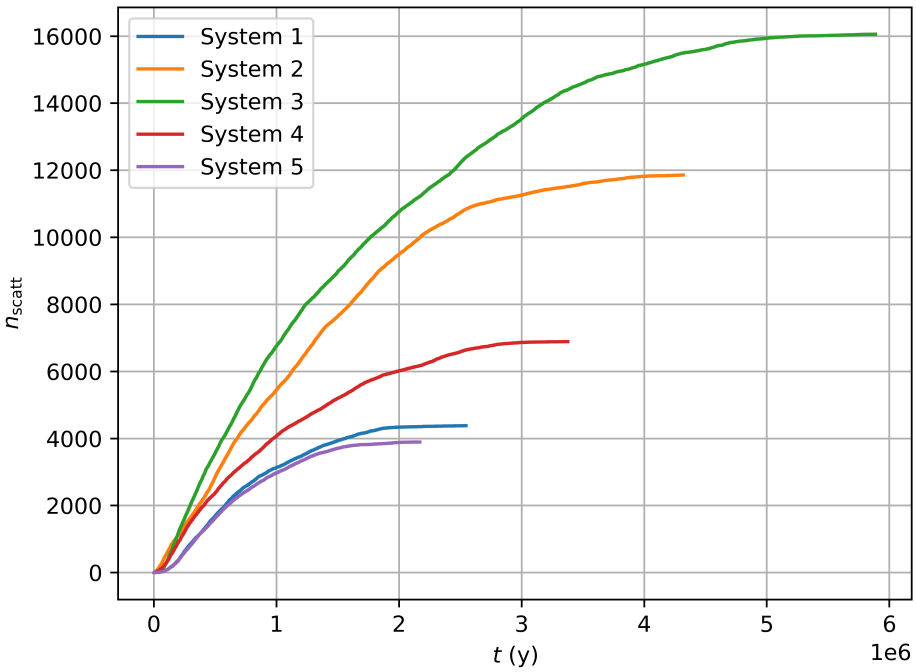

Figure 4.7: For five simulations with $\epsilon_{\max} = 0.2$, the total number of scatterings n_{scatt} is plotted versus the time t in years. Other relevant parameters are distributed as described in Table 3.1. The simulations stopped when the next scattering was more than 10^5y in the future

To further research the effects of many scatterings, we pick the system with the highest number of scatterings $n_{\max}$. In this case we will proceed using system 3 with $n_{\max} = 16057$. BIn Figure 4.8 the initial distributions of the parameters m, a, I and ϵ of the particles of system 3 are plotted with their theoretical distribution according to Table 3.1.

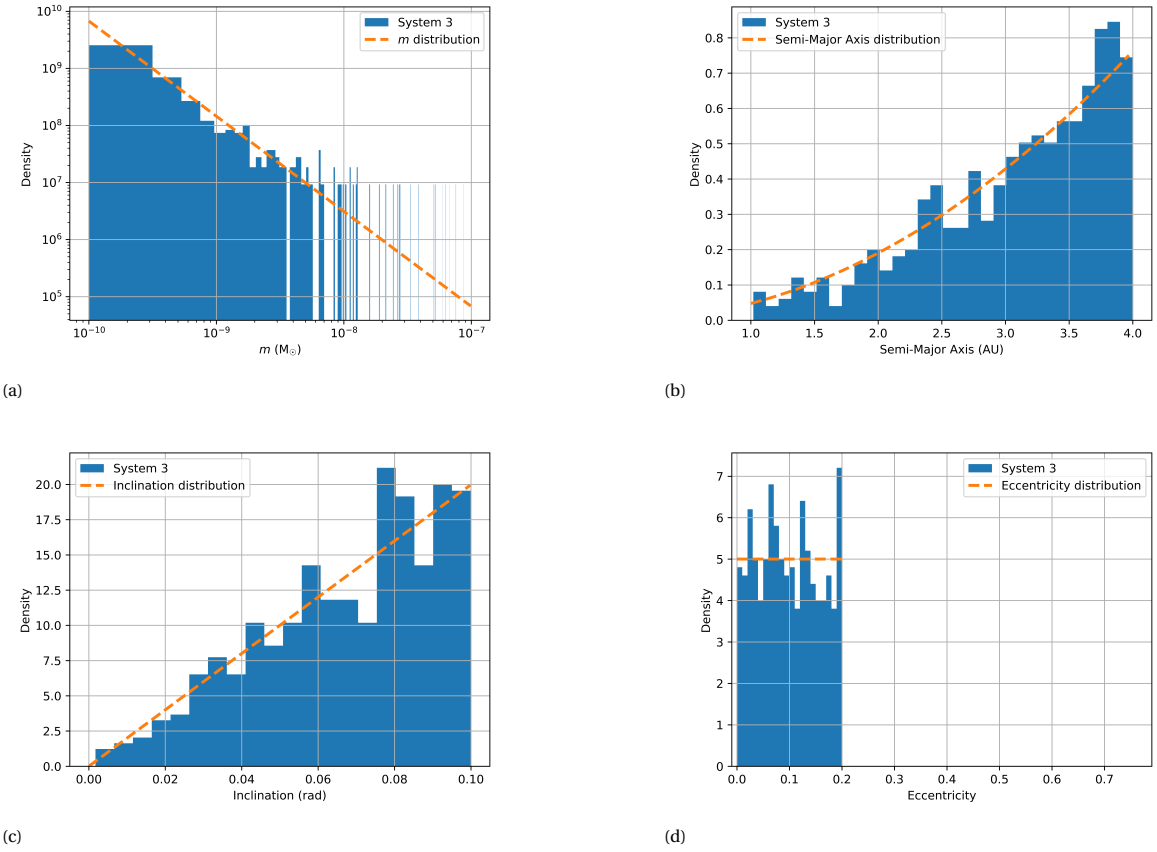

Figure 4.8: Density histograms showing the initial distributions of important parameters m, a, I and ϵ for system 2 for $\epsilon_{\max} = 0.1$. The orange lines indicate theoretical distributions from which the values for m_i, a_i, I_i and ϵ_i were generated for every particle $1 \leq i \leq 500$ using the formulas found in Table 3.1. (a): Density histogram log-log plot of the planetary masses m_i ($M_\odot$). (b) Density histogram plot of the Semi-Major Axis a_i (AU). (c) Density histogram plot of the Inclination I_i (rad). (d) Density histogram plot of the Eccentricity ϵ_i.

In order to showcase the effect of scatterings on the distribution of the eccentricity ϵ, the eccentricity distribution of the particles of system 3 is plotted at the start ($n_{\text{scatt}} = 0$) and at the end of the simulation ($n_{\text{scatt}} = n_{\text{max}}$). In Figure 4.9 we compare the eccentricity distribution in the initial and final state of system 3.

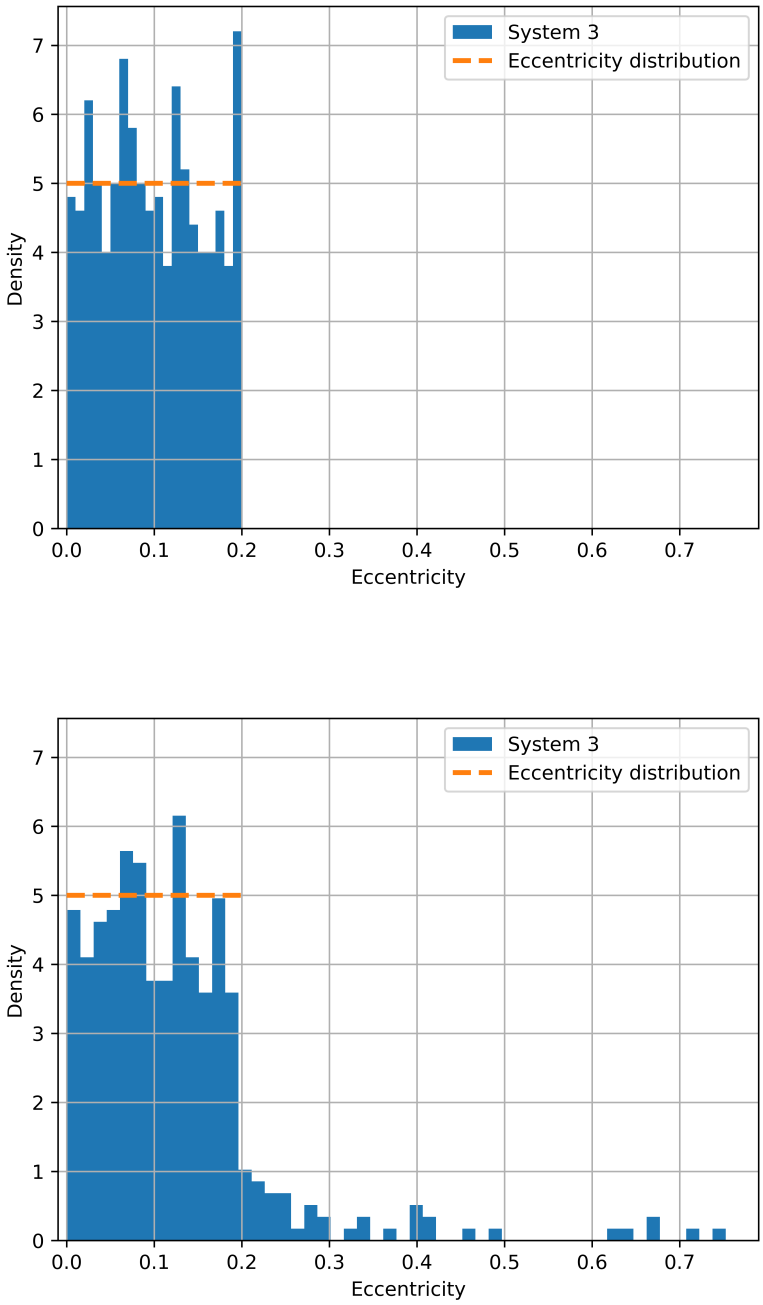

Figure 4.9: Above: Density histogram of the eccentricity of the initial particles in system 3. The orange line indicates the theoretical distribution used to generate ϵ_i found in Table 3.1. Below: Density histogram of the eccentricity of the final particles in system 3 with $n_{\text{scatt}} = n_{\text{max}} = 16057$. Here, the orange line of the initial eccentricity distribution is still drawn to more clearly showcase the change in distribution. Note that the total amount of planets is lower in the final state due to ejections.

To get an idea of the shape and distribution of the orbits of particles in system 3, both in the initial and final state, astronomy commonly uses (ϵ, a) plots. In Figure 4.10, we see a scatter-plot of the particles of system 3 in its final state.

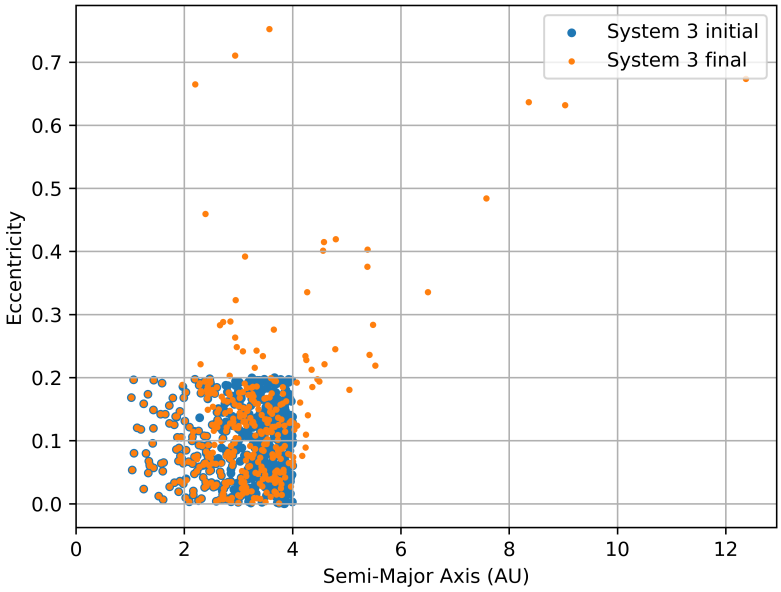

Figure 4.10: (ϵ, a) scatterplot of the particles in the final state of system 3 ($n_{\text{scatt}} = n_{\max} = 16057$). Note that the particles are no longer contained by the box $[a_{\min}, a_{\max}] \times [\epsilon_{\min}, \epsilon_{\max}]$. An orange dot on top of a blue dot means that that particle still has the same eccentricity and semi-major axis as in its initial state, indicating that it was not involved in any scattering events. We see that below 3AU, most particles have not been scattered, while above 3AU many particles have been scattered into high eccentric orbits.

As can be seen in the report made by Jort Koks [9], the simulations go through an initial phase where the scatter frequency is increasing. This is showcased for all systems in Figure 4.11.

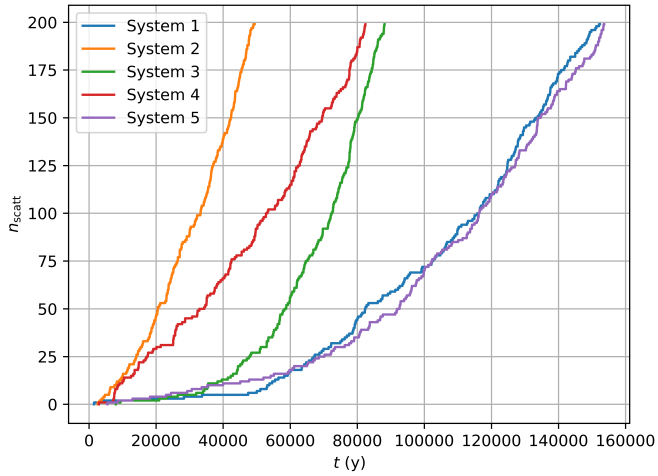

Figure 4.11: n_{scatt} plotted versus the time t in years for $n_{\text{scatt}} \leq 200$ for all systems with $\epsilon_{\text{max}} = 0.2$. $n_{\text{scatt}} = 200$ was chosen due to all simulated systems entering a phase of roughly constant scatter frequency after this scatter count. Some simulations take longer to enter this linear phase of the graph, while other systems start off almost linear already.

After $n_{\text{scatt}} = 200$, all systems go through a roughly linear period of growth. All systems exhibit a trend of decaying growth for $n_{\text{scatt}} \geq 200$, to which a curve can be fitted. The curve that most closely matches the shapes of the systems' (t, n_{scatt}) plots is $n_{\text{scatt}}(t) = n_{\text{max}} - ae^{-t/\tau}$. In Figure 4.12 the resulting curve-fit for system 3 can be found, fitted to values $200 \leq n_{\text{scatt}} \leq n_{\text{max}}$.

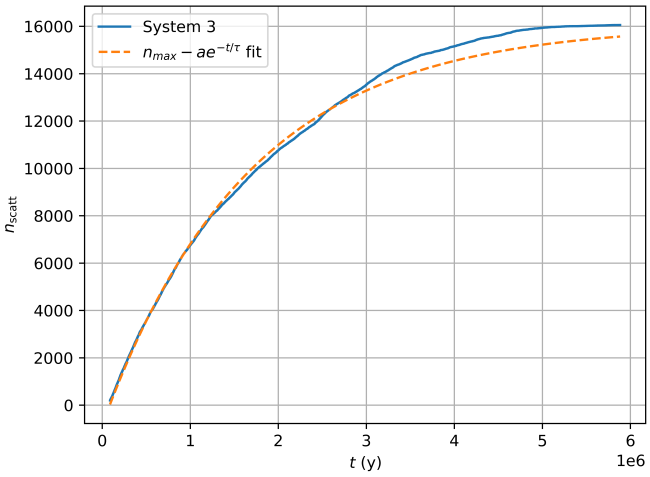

Figure 4.12: Number of scatterings of system 3 ($200 \leq n_{\text{scatt}} \leq n_{\text{max}} = 16057$) plotted versus the time t in years. The dashed orange line represents the results of a curve of shape $n_{\text{scatt}}(t) = n_{\text{max}} - ae^{-t/\tau}$ fitted to the data. n_{max} can only be determined after the simulation has been fully executed. The resulting fit parameters are $a = 16903 \pm 6$ and $\tau = (1660 \pm 1) \cdot 10^3$y.

4.3. Maximum eccentricity of 0.4

In Figure 4.13, 5 simulations with $\epsilon_{\max} = 0.4$ are shown, plotting the total scatter count n_{scatt} versus the time t in years.

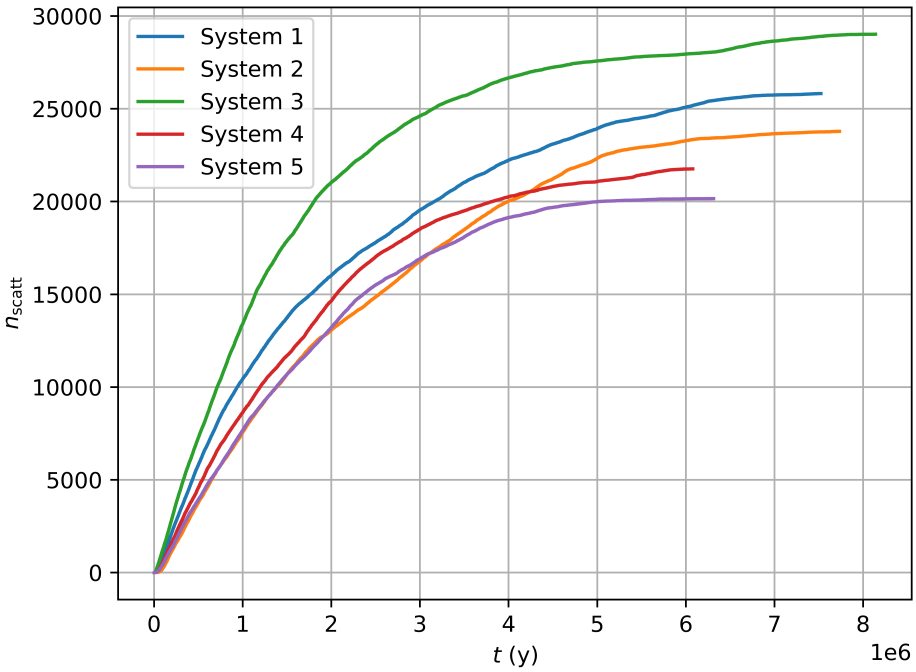

Figure 4.13: For five simulations with $\epsilon_{\max} = 0.4$, the total number of scatterings n_{scatt} is plotted versus the time t in years. Other relevant parameters are distributed as described in Table 3.1. The simulations stopped when the next scattering was more than 10^5y in the future

To further research the effects of many scatterings, we pick the system with the highest number of scatterings $n_{\max}$. In this case we will proceed using system 3 with $n_{\max} = 29017$. In Figure 4.14 the initial distributions of the parameters m, a, I and ϵ of the particles of system 3 are plotted with their theoretical distribution according to Table 3.1.

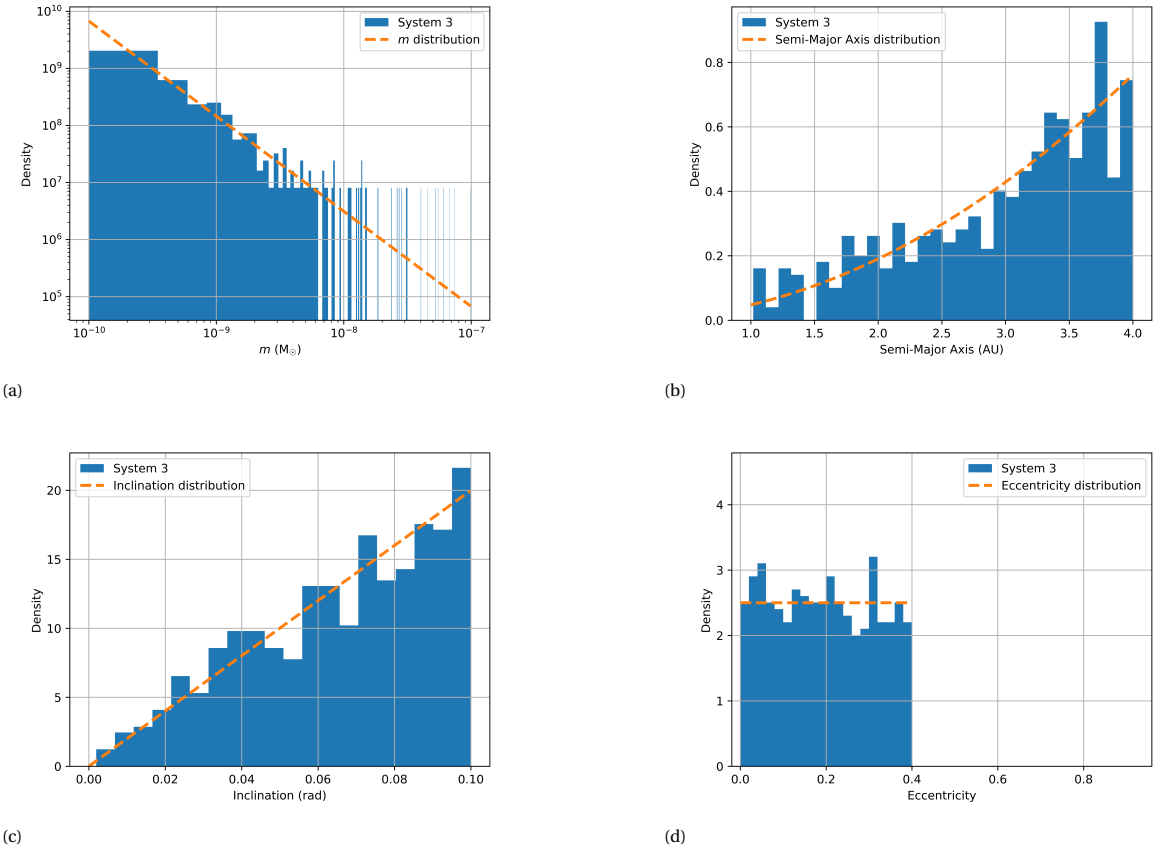

Figure 4.14: Density histograms showing the initial distributions of important parameters m, a, I and ϵ for system 3 for $\epsilon_{\max} = 0.4$. The orange lines indicate theoretical distributions from which the values for m_i, a_i, I_i and ϵ_i were generated for every particle $1 \leq i \leq 500$ using the formulas found in Table 3.1. (a): Density histogram log-log plot of the planetary masses m_i ($M_\odot$). (b) Density histogram plot of the Semi-Major Axis a_i (AU). (c) Density histogram plot of the Inclination I_i (rad). (d) Density histogram plot of the Eccentricity ϵ_i.

In order to showcase the effect of scatterings on the distribution of the eccentricity ϵ, the eccentricity distribution of the particles of system 3 is plotted at the start ($n_{\text{scatt}} = 0$) and at the end of the simulation ($n_{\text{scatt}} = n_{\text{max}}$). In Figure 4.15 we compare the eccentricity distribution in the initial and final state of system 3.

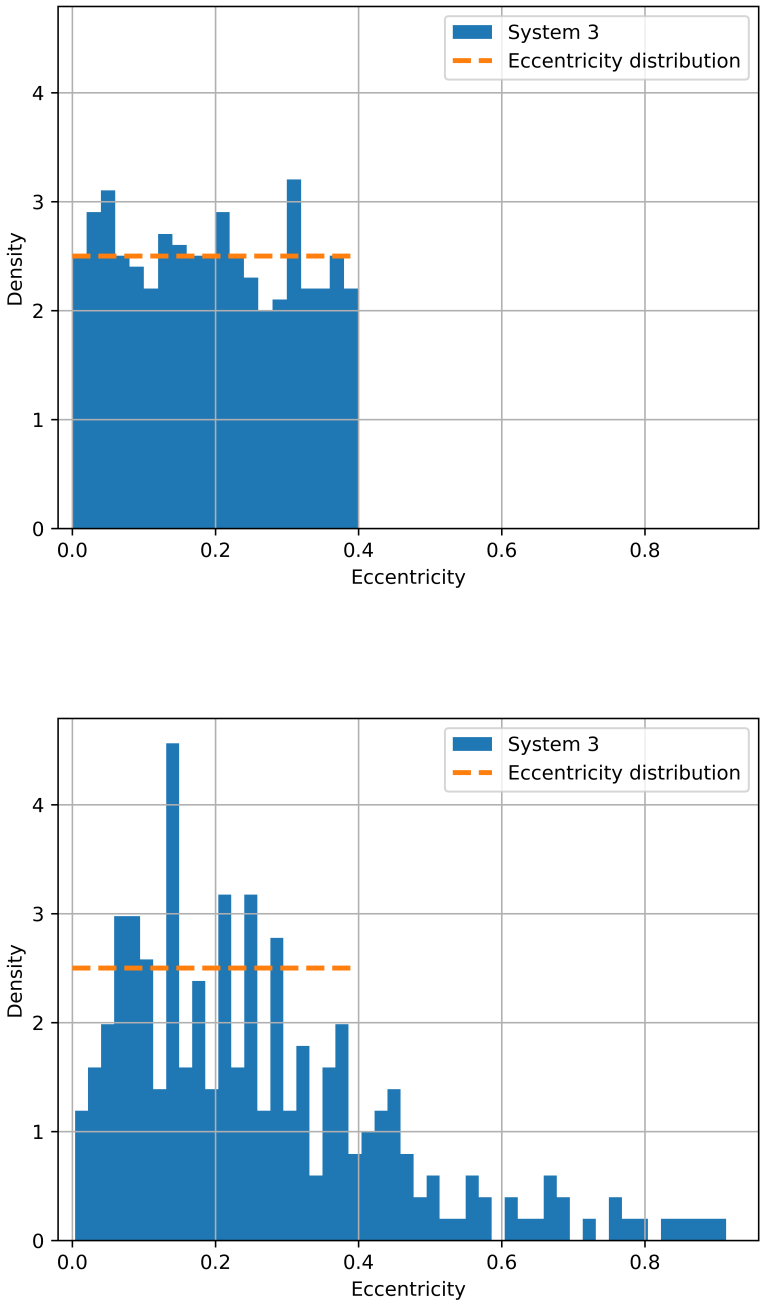

Figure 4.15: Above: Density histogram of the eccentricity of the initial particles in system 3. The orange line indicates the theoretical distribution used to generate ϵ_i found in Table 3.1. Below: Density histogram of the eccentricity of the final particles in system 3 with $n_{\text{scatt}} = n_{\text{max}} = 29017$. Here, the orange line of the initial eccentricity distribution is still drawn to more clearly showcase the change in distribution. Note that the total amount of planets is lower in the final state due to ejections.

To get an idea of the shape and distribution of the orbits of particles in system 3, both in the initial and final state, astronomy commonly uses (ϵ, a) plots. In Figure 4.16, we see a scatter-plot of the particles of system 3 in its final state.

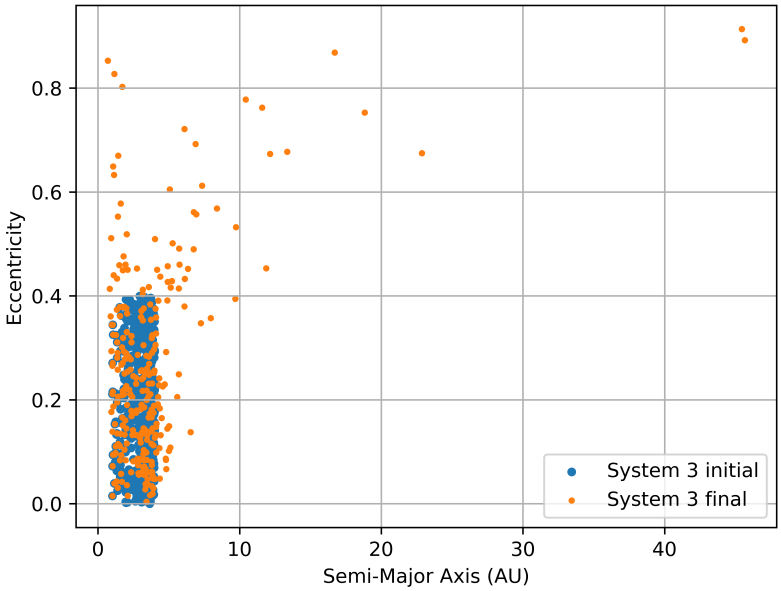

Figure 4.16: (ϵ, a) scatterplot of the particles in the final state of system 3 ($n_{\text{scatt}} = n_{\max} = 29017$). Note that the particles are no longer contained by the box $[a_{\min}, a_{\max}] \times [\epsilon_{\min}, \epsilon_{\max}]$. An orange dot on top of a blue dot means that that particle still has the same eccentricity and semi-major axis as in its initial state, indicating that it was not involved in any scattering events.

Since Figure 4.16 does not clearly visualize what happens in the domain of the initial simulation values $a \times \epsilon = [0,4] \times [0,0.4]$, Figure 4.17 zooms in on this domain which lets us easily see what particles were involved in a scatter event.

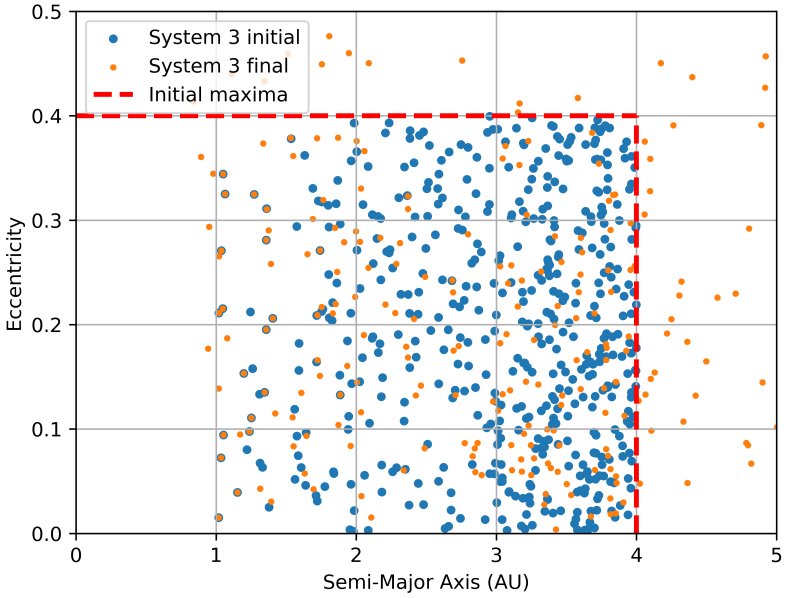

Figure 4.17: (ϵ, a) scatterplot of the particles in the final state of system 3 ($n_{\text{scatt}} = n_{\max} = 29017$). The minimum and maximum values of both ϵ and a form a box that all initial particles are contained by. This box is $[a_{\min}, a_{\max}] \times [\epsilon_{\min}, \epsilon_{\max}]$. Due to the many scatterings that have taken place in system 3 ($n_{\max} = 29017$), particles have exited this box. An orange dot on top of a blue dot means that that particle still has the same eccentricity and semi-major axis as in its initial state, indicating that it was not involved in any scattering events.

As can be seen in the report made by Jort Koks [9], the simulations go through an initial phase where the scatter frequency is increasing. This is showcased for all systems in Figure 4.18.

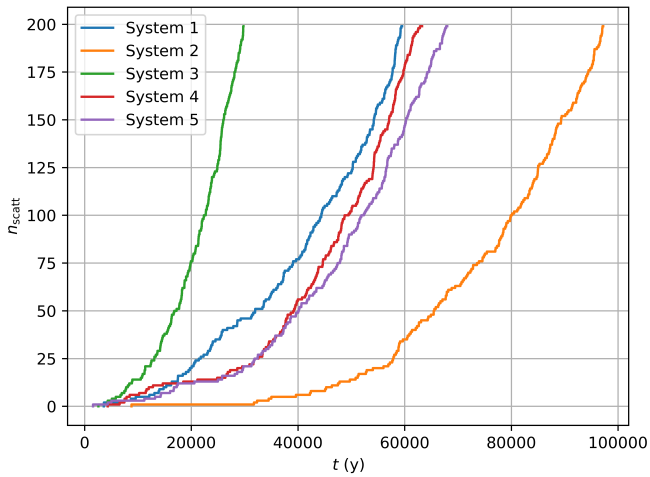

Figure 4.18: n_{scatt} plotted versus the time t in years for $n_{\text{scatt}} \leq 200$ for all systems with $\epsilon_{\text{max}} = 0.4$. $n_{\text{scatt}} = 200$ was chosen due to all simulated systems entering a phase of roughly constant scatter frequency after this scatter count. Some simulations take longer to enter this linear phase of the graph, while other systems start off almost linear already.

After $n_{\text{scatt}} = 200$, all systems go through a roughly linear period of growth. All systems exhibit a trend of decaying growth for $n_{\text{scatt}} \geq 200$, to which a curve can be fitted. The curve that most closely matches the shapes of the systems' (t, n_{scatt}) plots is $n_{\text{scatt}}(t) = n_{\text{max}} - ae^{-t/\tau}$. In Figure 4.19 the resulting curve-fit for system 3 can be found, fitted to values $200 \leq n_{\text{scatt}} \leq n_{\text{max}}$.

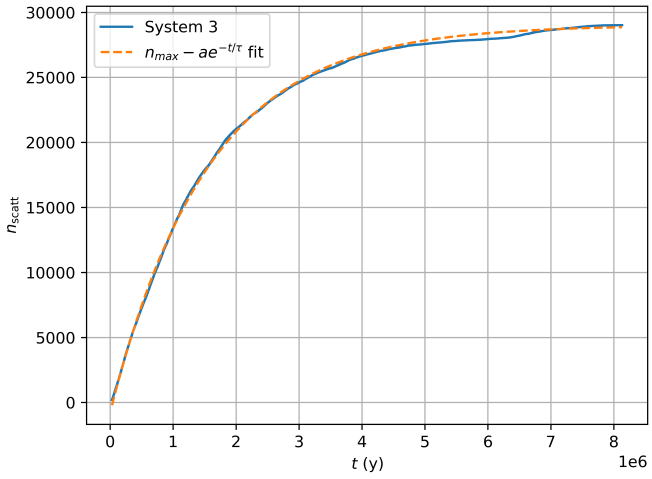

Figure 4.19: Number of scatterings of system 3 ($200 \leq n_{\text{scatt}} \leq n_{\text{max}} = 29017$) plotted versus the time t in years. The dashed orange line represents the results of a curve of shape $n_{\text{scatt}}(t) = n_{\text{max}} - ae^{-t/\tau}$ fitted to the data. n_{max} can only be determined after the simulation has been fully executed. The resulting fit parameters are $a = 29802 \pm 3$ and $\tau = (15483 \pm 3) \cdot 10^2$y.

4.4. Comparing different values for ϵ_{max}

In Table 4.1 the results for 5 simulations per value of $\epsilon_{\text{max}} \in \{0.1, 0.2, 0.4\}$ are compared. Using the fact that $n_{\text{scatt}}(t) = n_{\text{max}} - ae^{-t/\tau}$ can be rewritten as $n_{\text{scatt}}(t) = n_{\text{max}}\left(1 - e^{(t-t_0)/\tau}\right)$ without loss of generality with $t_0 = \tau \ln(a/n_{\text{max}})$, we can find a time offset t_0 for every simulation. The increases in final eccentricity due to scatter events are shown in Table 4.2.

$\epsilon_{\max}$	$\langle n_{\max} \rangle$	$\langle a \rangle$	$\langle t_0 \rangle$ (y)	$\langle \tau \rangle$ (y)
0.1	$(1.9 \pm 0.6) \cdot 10^3$	$(2.6 \pm 0.5) \cdot 10^3$	$(1.4 \pm 0.6) \cdot 10^5$y	$(4.3 \pm 0.9) \cdot 10^5$y
0.2	$(9 \pm 5) \cdot 10^3$	$(1.0 \pm 0.5) \cdot 10^4$	$(1.1 \pm 0.4) \cdot 10^5$y	$(1 \pm 0.4) \cdot 10^6$y
0.4	$(2.4 \pm 0.3) \cdot 10^4$	$(2.5 \pm 0.3) \cdot 10^4$	$(0.8 \pm 0.5) \cdot 10^5$y	$(1.8 \pm 0.3) \cdot 10^6$y

Table 4.1: Table with the mean values of various variables acquired by fitting a curve to the data showcased in Figures 4.1, 4.7 and 4.13. 3 values for $\epsilon_{\max}$ were used, running 5 simulations per value.

$\epsilon_{\max}$	$\langle n_{\max} \rangle$	$\langle \epsilon \rangle_f$	$\langle \epsilon \rangle_f$ / $\langle \epsilon \rangle_i$
0.1	$(1.9 \pm 0.6) \cdot 10^3$	$(5.2 \pm 0.1) \cdot 10^{-2}$	1.04 ± 0.02
0.2	$(9 \pm 5) \cdot 10^3$	$(1.06 \pm 0.08) \cdot 10^{-1}$	1.06 ± 0.08
0.4	$(2.4 \pm 0.3) \cdot 10^4$	$(2.2 \pm 0.2) \cdot 10^{-1}$	1.1 ± 0.1

Table 4.2: Table with the mean eccentricity of the final state of multiple simulations. 3 values per value of $\epsilon_{\max}$ were used, running 5 simulations per value for a total of 15 simulations. Since ϵ is uniformly distributed, $\langle \epsilon \rangle_i = \epsilon_{\max}/2$

5

Discussion

In this section, the three main questions will be discussed. Furthermore, the shortcomings and oversights of the Keplerian model and algorithm [11] will also be discussed. Since the research mainly focused on simulating the generated systems until they became practically stable and then analyzing the results, we did not go into the research with any expectations stemming from theory.

1. *How does the initial maximum eccentricity ϵ_{max} of a system relate to the total number of scatterings n_{max} needed for a system to become effectively stable?*

   For the values of $\epsilon_{\max} \in \{0.1, 0.2, 0.4\}$, 5 simulations were ran as can be seen in Figures 4.1, 4.7 and 4.13. The value of $\langle n_{\max} \rangle$ increases as the maximum eccentricity $\epsilon_{\max}$ increases as can be seen in Table 4.2. This can be explained by an increasing eccentricity resulting in more orbits overlapping each other, as the elliptical orbits get "flattened out" due to the increased eccentricity. A lower eccentricity means that orbits are more circular, meaning that the difference in semi-major axis a between two objects needs to be smaller for spheres of influence to intersect. The chance of this happening is low, as can be observed in Figure 4.2b.

2. *Is the total number of occurred scatterings n_{scatt} related to the elapsed time t? If so, can we find a general closed form formula $n_{scatt}(t)$ to fit to the data?*

   As can be observed in Figures 4.6, 4.12 and 4.19, there is a closed form formula for $n_{\text{scatt}}(t)$ that accurately fits the data when fitted to $n_{\text{scatt}} \geq 200$. This formula is $n_{\text{scatt}}(t) = n_{\max} - ae^{-t/\tau}$, where a is a dimensionless parameter that has a value close to $n_{\max}$, and τ is the time constant of the simulation in years. As $n_{\max}$ increases, the error of the fit decreases as can be seen when comparing the standard deviation for the fit parameters a and τ in the captions of Figures 4.6, 4.12 and 4.19. When rewriting the formula to $n_{\text{scatt}}(t) = n_{\max}\left(1 - e^{(t-t_0)/\tau}\right)$ and looking at the value for t_0 as seen in Table 4.1, we see that t_0 is decreasing. This implies that for $n_{\text{scatt}} \leq 200$, we have a higher rate of collision as the $\epsilon_{\max}$ increases . We also see that $\langle a \rangle$ approaches $\langle n_{\max} \rangle$ as $\epsilon_{\max}$ increases, which makes sense when you consider that in $n_{\text{scatt}}(t) = n_{\max}\left(1 - e^{(t-t_0)/\tau}\right)$, $n_{\max}$ is the asymptote that the function $n_{\text{scatt}}(t)$ approaches as it becomes practically stable. The timescale $\langle \tau \rangle$ also increases as $\epsilon_{\max}$ increases since it takes more time to reach an effectively stable configuration. This implies that a higher value of $\epsilon_{\max}$ results in a longer simulation runtime.

3. *Can the total number of scatterings required for practical stability n_{max} be predicted based on the simulation parameters?*

   From Figures 4.1, 4.7, 4.13 and Table 4.2, we see that for the 5 simulations per $\epsilon_{\max}$, the value of $n_{\max}$ varies wildly. This is due to the random and chaotic nature of the N-body system and the algorithm used to evolve it throughout time. Since just a single collision mutates the orbital parameters of 1 or 2 planets, this starts a domino effect where the mutated planet(s) now also interact with other planets. This implies that we can not predict $n_{\max}$ based on the simulation parameters, or even give an interval in which $n_{\max}$ lies. By running more simulations per value of $\epsilon_{\max}$, it could be possible to find a confidence interval

for the value of $n_{\max}$, however these values strongly depend on the simulation parameter values and are therefore specific to this set of parameter values.

Early behavior of initial state

As can be seen in Figure 4.5, Figure 4.11 and Figure 4.18, during the first 200 scatterings there is an increasing rate of collision $\frac{dn_{\text{scatt}}}{dt}$. However, the system was generated to be a uniformly homogeneous disk. This implies that we do not expect $\frac{dn_{\text{scatt}}}{dt}$ to be initially increasing. It is not clear why the system always starts with an increasing rate of collision, but it could have to do with the fact that the system is randomly generated. Physical systems do not suddenly come into existence, and evolve towards this initial state, whereas in a simulation the system is artificially created at an initial time t.

Arbitrary cutoff for formula fit

The cutoff for the early behavior of the initial state is arbitrarily set at $n_{\text{scatt}} = 200$, without any further motivation besides empirical observations. This therefore is not supported by any theory or formulae, and the exact cutoff for the early behavior can vary depending on the value of $\epsilon_{\max}$ or even the random generation of a simulation. More simulations would need to be ran for the minimum value of $\epsilon_{\max}$ to figure out the minimal n_{scatt} needed.

Elastic gravitational scattering of close encounters

For close encounters, we simulate until the time t' of MOID (minimal orbit intersection distance). Once we reach t', the new orbital parameter values of the planets involved are determined and updated to this new set of parameters. This of course is not realistic, as it assumes that the planets do not exert any gravitational force upon each other as they are getting closer and closer to the point of MOID. It therefore neglects interplanetary gravitational forces up to a certain point, but this also has greater consequences for the simulation itself due to it's chaotic nature. If these interplanetary gravitational forces were taken into account during the approach to the MOID, what would be simulated as a close encounter could physically end up as a direct collision. Due to the chaotic nature of these systems, we could see significantly different results.

Linearisation of collision detection

To simplify a lot of the calculations necessary to run the algorithm and determine the evolution of the Keplerian system, interactions such as the gravitational scattering, direct collision and calculation of the MOID are linearized. By calculating the MOID, we check if planets will even be involved in a scattering event. Due to the chaotic nature of an N-body system, these seemingly inconsequential approximations quickly add up.

Inelastic direct encounters

It is assumed that any direct encounter between 2 bodies results in the merging of the bodies involved, with no encounters resulting in fragmentation of a body. Another assumption made is that the direct collisions don't result in any change in axial spin of the merged planet, since the planets do not have a spin parameter. Spin of course requires energy, which would mean that the resulting orbital parameter values would differ from the collision without spin. It is also assumed that the bodies are spherical, which of course would not always be the case after a collision between two bodies.

Planet ejection/destruction after scatter event

It is possible for scatter events of both kinds (close encounter and direct collision) to result in the ejection/destruction of a planet. In the case of a destruction, the orbit would result in hitting the central mass, whereas an ejection means that the planet no longer orbits the central mass. In both cases, a planet could undergo interactions with other planets as it flies into the central mass/exits the solar system. This however is not accounted for in the simulation. The simulation also does not take into account for the conservation of (angular) momentum when such an ejection/destruction occurs.

Laplace sphere of influence

The Laplace sphere of influence $s^{\text{inf}} = r_1 \left(\frac{m}{M}\right)^{2/5}$ is not the only theoretical sphere of influence that determines when the gravitational pull of the smaller body exceeds that of the central mass. The Laplace sphere is also approximated to be spherical and uses an approximation resulting in a slightly bigger radius. The Laplace sphere of influence decides when planets are close enough to meaningfully scatter each other through gravity,

which combined with the chaotic nature of the N-body system heavily influences its evolution throughout time.

Long-range gravitational interactions

The simulation does not take into account the effects of long-range gravitational interactions between objects. An improvement to the simulation would be to take these gravitational forces into account. For an asteroid belt there are not many significantly heavier masses, but as the relative difference between the lightest and heaviest mass increases, the influence of the long-range gravitational interactions also increases. This has an effect on the orbits of all planets, attracting the objects and their orbitals as time progresses.

Random nature of initial state generation

Due to the random nature of the generation of the initial states and chaotic nature of the algorithm, it is hard to predict what the exact evolution of the (n_{scatt}, t) will look like. It is also not possible to fit a closed formula function $n(t)$ before the value of $n_{\max}$ is determined by a simulation. This means that the simulation needs to be ran until completion before we can have any clue about its properties.

6

Conclusion

The goal of this research was to answer three questions related to the evolution of a generated initial N-body Keplerian system, similar to an asteroid belt. Since the evolutions of the simulations completely depend on the simulation parameters as described in Table 3.2 and the randomness, exact values of fit parameters or values of $n_{\max}$ are not very useful. What is valuable however, is the patterns and correlations that can be deduced from varying initial simulation parameters. We have shown that the number of total scatterings $n_{\max}$ required for an effectively stable configuration varies significantly for identical initial simulation parameters. The value of $\langle n_{\max} \rangle$ does increase as $\epsilon_{\max}$ increases. Despite this variance, there exists a closed form formula $n_{\text{scatt}}(t) = n_{\max}\left(1 - e^{(t-t_0)/\tau}\right)$ that accurately fits the data for every simulation.

Further research could vary the inclination $I_{\max}$ and semi-major axis $[a_{\min}, a_{\max}]$ to see if these are also related to $n_{\max}$. Despite the fact that the inclination $I_{\max}$ and semi-major axis $[a_{\min}, a_{\max}]$ are distributed in such a way that the distribution always results in a uniform homogeneous disc, I suspect that a higher value of $I_{\max}$ and larger interval $[a_{\min}, a_{\max}]$ will result in a lower $\langle n_{\max} \rangle$. This would be due to the sphere of influence staying the same radius (same mass distribution), as the total volume of allowed space increases.

References

[1] R. A. Adams. *Student Solutions Manual to Calculus: A complete course, eighth edition by Robert A. Adams, Christopher Essex*, page 666. Pearson, 2014.

[2] Richard H Battin. *An introduction to the mathematics and methods of astrodynamics*, page 395. Aiaa, 1999.

[3] Irene Cavallari, Clara Grassi, Giovanni F. Gronchi, Giulio Baù, and Giovanni B. Valsecchi. A dynamical definition of the sphere of influence of the earth. *Communications in Nonlinear Science and Numerical Simulation*, 119:107091, 2023. ISSN 1007-5704. doi: https://doi.org/10.1016/j.cnsns.2023.107091. URL https://www.sciencedirect.com/science/article/pii/S1007570423000096.

[4] G.A. Chebotarev. Gravitational spheres of the major planets, moon and sun. *Soviet Astronomy*, 1964.

[5] D. R. Davis, D. D. Durda, F. Marzari, A. Campo Bagatin, and R. Gil-Hutton. Collisional Evolution of Small-Body Populations. In W. F. Bottke, Jr., A. Cellino, P. Paolicchi, and R. P. Binzel, editors, *Asteroids III*, pages 545–558. 2002.

[6] J.F. Koks. Simulation of gravitational scatterings in n -body kepler systems, Jan 2023. URL https://repository.tudelft.nl/record/uuid:084af7e7-68bd-4cdb-8bf3-31d478690dd3.

[7] Lasunncty. Keplerian orbital elements, 2007. URL https://en.wikipedia.org/wiki/Kepler_orbit#/media/File:Orbit1.svg. Orbit1.svg.

[8] Tom Logsdon. *Orbital Mechanics: Theory and Applications*. Wiley, 1998.

[9] M. Moorlag. A keplerian method for collision detection in protoplanetary disk simulations, Sep 2022. URL https://repository.tudelft.nl/file/File_516c8ace-a492-4833-b72b-9bf0c6c893d6?preview=1.

[10] Thunkii. Kuiper belt eccentricity, 2007. URL https://commons.wikimedia.org/wiki/File:Kuiper-belt-eccentricity.svg.

[11] P. M. Visser. Collision detection for n-body kepler systems. *Astronomy &; Astrophysics*, 669:A97, January 2023. ISSN 1432-0746. doi: 10.1051/0004-6361/202243754. URL http://dx.doi.org/10.1051/0004-6361/202243754.